

# SCALE FORMATION OF SOFC METALLIC INTERCONNECTS IN COAL SYNGAS

by

**Jingpeng Wang**

B.S., Xi'an University of Technology, 2002

M.S., Institute of Metal Research, CAS, 2005

Submitted to the Graduate Faculty of  
the School of Engineering in partial fulfillment  
of the requirements for the degree of  
Master of Science

University of Pittsburgh

2007

UNIVERSITY OF PITTSBURGH

SCHOOL OF ENGINEERING

This thesis was presented

by

Jingpeng Wang

It was defended on

November 30, 2007

and approved by

Scott X. Mao, Professor, Mechanical Engineering and Materials Science Department

Sung Kwon Cho, Assistant Professor, Mechanical Engineering and Materials Science Department

Kevin P. Chen, Assistant Professor, Electrical and Computer Engineering Department

Thesis Advisor: Scott X. Mao, Professor, Mechanical Engineering and Materials Science

Department

Copyright © by Jingpeng Wang

2007

# **SCALE FORMATION OF SOFC METALLIC INTERCONNECTS IN COAL SYNGAS**

Jingpeng Wang, M.S.

University of Pittsburgh, 2007

Planar solid oxide fuel cells (SOFCs) which can use coal syngas as the fuel and stainless steels in their construction have attracted considerable interest, due to the high power densities and cost-effective manufacturing. However, the components of SOFCs work under a long-term, high temperature corrosive atmosphere, which places a lot of stringent requirements on the materials of the components. For interconnects, since they are simultaneously exposed to air on the cathode side and to fuel on the anode side, the materials must have good oxidation resistance, as well as other electric and mechanical properties. Although extensive research has been done to examine the oxidation behaviors of many potential interconnect materials in air, hydrogen and dual-atmosphere, little oxidation information of these materials in a coal syngas environment is available. Because the oxidation properties of materials in different media are quite different, evaluating the oxidation behavior of these potential interconnect materials in coal syngas is available.

In the present work, the oxidation properties of Fe-based ferritic alloys Crofer 22 APU, E-Brite, AISI 430 and a Ni-based alloy Haynes 230 isothermally exposed in coal syngas at 800 °C for 100 hours and 500 hours were studied. Moreover, the effects of pre-oxidized coating and cladding on the oxidation properties of the materials in coal syngas at high temperatures were investigated and both of them could significantly improve the oxidation resistance.

## TABLE OF CONTENTS

<b>TABLE OF CONTENTS .....</b>	<b>V</b>
<b>LIST OF TABLES .....</b>	<b>VIII</b>
<b>LIST OF FIGURES .....</b>	<b>IX</b>
<b>ACKNOWLEDGMENTS .....</b>	<b>XIII</b>
<b>1.0 INTRODUCTION.....</b>	<b>1</b>
<b>2.0 BACKGROUND .....</b>	<b>3</b>
<b>2.1 FUEL CELL.....</b>	<b>3</b>
<b>2.1.1 Components and operating principle .....</b>	<b>3</b>
<b>2.1.2 Types of fuel cells.....</b>	<b>4</b>
<b>2.1.3 Advantages and applications .....</b>	<b>6</b>
<b>2.2 SOLID OXIDE FUEL CELLS (SOFCs) .....</b>	<b>7</b>
<b>2.2.1 Operating principle .....</b>	<b>7</b>
<b>2.2.2 Design of SOFCs .....</b>	<b>8</b>
<b>2.2.3 Advantages .....</b>	<b>9</b>
<b>2.3 INTERCONNECTS OF SOFCs.....</b>	<b>9</b>
<b>2.3.1 The roles of interconnects .....</b>	<b>9</b>
<b>2.3.2 The requirements.....</b>	<b>10</b>
<b>2.3.3 The materials for interconnects.....</b>	<b>11</b>

<b>2.4</b>	<b>INTRODUCTION OF HIGH-TEMPERATURE OXIDATION .....</b>	<b>14</b>
2.4.1	Thermodynamics .....	15
2.4.2	Mechanism of oxidation .....	16
2.4.3	Oxidation of alloys.....	18
2.4.4	Oxidation of interconnects.....	19
2.4.5	Protection of interconnects .....	21
<b>3.0</b>	<b>MOTIVATION AND OBJECTIVE OF THE STUDY .....</b>	<b>23</b>
<b>4.0</b>	<b>EXPERIMENTAL PROCEDURES .....</b>	<b>24</b>
<b>4.1</b>	<b>MATERIALS .....</b>	<b>24</b>
4.1.1	Crofer 22 APU .....	24
4.1.2	E-Brite.....	25
4.1.3	Haynes 230.....	25
4.1.4	AISI 430.....	26
<b>4.2</b>	<b>MATERIALS PREPARATION.....</b>	<b>26</b>
<b>4.3</b>	<b>CHARACTERIZATION .....</b>	<b>27</b>
<b>5.0</b>	<b>RESULTS AND DISCUSSION .....</b>	<b>28</b>
<b>5.1</b>	<b>CROFER 22 APU .....</b>	<b>28</b>
5.1.1	Exposed in coal syngas at 800 °C for 100 hours.....	28
5.1.2	Exposed in coal syngas at 800 °C for 500 hours.....	30
5.1.3	Pre-oxidized samples .....	34
<b>5.2</b>	<b>E-BRITE.....</b>	<b>40</b>
5.2.1	Exposed in coal syngas for 100 hours .....	40
5.2.2	Exposed in coal syngas for 500 hours .....	42

<b>5.3</b>	<b>HAYNES 230.....</b>	<b>44</b>
5.3.1	Exposed in coal syngas for 100 hours .....	44
5.3.2	Exposed in coal syngas for 500 hours .....	45
5.3.3	Pre-oxidized samples .....	48
<b>5.4</b>	<b>CLAD MATERIALS.....</b>	<b>50</b>
5.4.1	E-Brite/Haynes 230.....	51
5.4.2	AISI 430/Haynes 230 .....	55
<b>5.5</b>	<b>SUMMARY AND DISCUSSION.....</b>	<b>60</b>
<b>6.0</b>	<b>CONCLUSION.....</b>	<b>64</b>
	<b>BIBLIOGRAPHY .....</b>	<b>66</b>

## LIST OF TABLES

<b>Table 2.1:</b> The main characteristics of different types of fuel cells.....	5
<b>Table 4.1:</b> Composition (in wt.%) of the selected alloys.....	24
<b>Table 5.1:</b> Main characteristic of the scales after oxidation in coal syngas at 800 °C for 500 hours.....	61

## LIST OF FIGURES

<b>Figure 2.1:</b> Schematic illustration of the operating principles of a fuel cell [9] .....	4
<b>Figure 2.2:</b> Ellingham diagram of some selected simple oxides. [23].....	17
<b>Figure 2.3:</b> Schematic diagram of the mechanism of oxidation [23].....	18
<b>Figure 2.4:</b> Weight change of ASL 528 during oxidation in air at 800-1000 °C [19] .....	20
<b>Figure 5.1:</b> SEM morphology of the surface of Crofer 22 APU exposed in coal syngas for 100 hours: (a) 5000X, (b) 20000X.....	28
<b>Figure 5.2:</b> XRD pattern of scales grown on Crofer 22 APU exposed in coal syngas for 100 hours.....	29
<b>Figure 5.3:</b> EDX linear analysis of the cross section of the oxide scale of Crofer 22 APU exposed in coal syngas for 100 hours .....	30
<b>Figure 5.4:</b> SEM morphology of the surface of Crofer 22APU exposed in coal syngas for 500 hours: (a) 5000X, (b) 20000X.....	31
<b>Figure 5.5:</b> XRD pattern of scales grown on Crofer 22 sample exposed in coal syngas for 500 hours.....	32
<b>Figure 5.6:</b> (a) Cross-sectional EDX linear analysis of the oxide scale of Crofer 22 APU exposed in coal syngas for 500 hours; (b) SEM morphology of the cross section.....	33
<b>Figure 5.7:</b> SEM morphology of the surface of pre-oxidized Crofer 22 APU sample:.....	36
<b>Figure 5.8:</b> EDX point analysis of the scale of Crofer 22 APU after further oxidation in air for 100 hours.....	36
<b>Figure 5.9:</b> SEM morphology of the surface of the pre-oxidized Crofer 22APU after further oxidation in air for 100 hours: (a) 5000X, (b) 20000X.....	37

<b>Figure 5.10:</b> SEM morphology of the surface of the pre-oxidized Crofer 22APU after further oxidation in syngas for 500 hours: (a) 2000X, (b) 20000X, (c) 20000X (an area without the short-fiber phase) .....	38
<b>Figure 5.11:</b> XRD pattern of scales grown on pre-oxidized Crofer 22 APU after further exposure in coal syngas for 500 hours .....	39
<b>Figure 5.12:</b> EDX linear analysis of the cross section of the oxide scale of pre-oxidized Crofer 22 APU after further exposure in syngas for 500 hours .....	39
<b>Figure 5.13:</b> SEM morphology of the surface of E-Brite after oxidation in coal syngas for 100 hours: (a) 5000X, (b) 20000X.....	41
<b>Figure 5.14:</b> XRD pattern of scales on E-Brite after oxidation in coal syngas for 100 hours .....	41
<b>Figure 5.15:</b> SEM morphology of the surface of E-Brite sample after oxidation in coal syngas for 500 hours: (a) 5000X, (b) 20000X .....	42
<b>Figure 5.16:</b> XRD pattern of scales grown on E-Brite after oxidation in coal syngas at 800 °C for 500 hours.....	43
<b>Figure 5.17:</b> (a) SEM morphology of the cross section of E-Brite exposed in coal syngas at 800 °C for 500 hours; (b) Cross-sectional EDX linear analysis. ....	43
<b>Figure 5.18:</b> SEM morphology of the surface of Haynes 230 sample after oxidation in coal syngas for 100 hours: (a) 5000X, (b) 20000X .....	44
<b>Figure 5.19:</b> XRD pattern of scales grown on Haynes 230 sample after oxidation in coal syngas at 800 °C for 100 hours .....	45
<b>Figure 5.20:</b> SEM morphology of the surface of Haynes 230 after oxidation in coal syngas for 500 hours: (a) 5000X, (b) 20000X.....	45
<b>Figure 5.21:</b> XRD pattern of scales grown on Haynes 230 after oxidation in coal syngas for 100 hours.....	46
<b>Figure 5.22:</b> (a) SEM morphology of the cross section of Haynes 230 exposed in coal syngas at 800 °C for 500 hours; (b) Cross-sectional linear EDX analysis. ....	47

<b>Figure 5.23:</b> SEM morphology of the surface of pre-oxidized Haynes 230 after further oxidation in coal syngas for 500 hours: (a) 5000X, (b) 20000X .....	48
<b>Figure 5.24:</b> XRD pattern of scales grown on pre-oxidized Haynes 230 after further oxidation in coal syngas for 500 hours .....	49
<b>Figure 5.25:</b> (a) SEM morphology of the cross section of pre-oxidized Haynes 230 sample after further oxidation in coal syngas for 500 hours; (b) Cross-sectional linear EDX analysis.	50
<b>Figure 5.26:</b> SEM morphology of the E-Brite side of the E-Brite/Haynes 230 clad sample after oxidation in coal syngas for 500 hours. ....	51
<b>Figure 5.27:</b> XRD pattern of scales grown at the E-Brite side of the E-Brite/Haynes 230 clad sample after oxidation in coal syngas for 500 hours.....	52
<b>Figure 5.28:</b> Cross-sectional EDX linear analysis at the E-Brite side of the E-Brite/Haynes 230 clad sample after oxidation in coal syngas for 500 hours.....	53
<b>Figure 5.29:</b> SEM morphology of the Haynes 230 side of the E-Brite/Haynes 230 clad sample after oxidation in coal syngas for 500 hours.....	53
<b>Figure 5.30:</b> XRD pattern of scales grown at the Haynes 230 side of the E-Brite/Haynes 230 clad sample after oxidation in coal syngas for 500 hours.....	54
<b>Figure 5.31:</b> Cross-sectional EDX linear analysis at the Haynes 230 side of the E-Brite/Haynes 230 clad sample after oxidation in coal syngas for 500 hours.....	54
<b>Figure 5.32:</b> SEM morphology of AISI 430 after oxidation in coal syngas at 800 °C for 500 hours: (a) clad with Haynes 230, (b) unclad.....	55
<b>Figure 5.33:</b> EDX linear analysis of unclad AISI 430 after oxidation in coal syngas for 500 hours.....	56
<b>Figure 5.34:</b> (a) Cross-sectional EDX linear analysis of the oxide scale at the AISI 430 side of the AISI 430/Haynes 230 clad sample exposed in coal syngas for 500 hours; (b) SEM morphology of the cross section .....	57
<b>Figure 5.35:</b> SEM morphology of the Haynes 230 side of the AISI 430/Haynes 230 clad sample after oxidation in coal syngas for 500 hours.....	58

**Figure 5.36:** XRD pattern of scales grown on the Haynes 230 side of the AISI 430/Haynes 230 clad sample after oxidation in coal syngas for 500 hours ..... 58

**Figure 5.37:** Cross-sectional EDX linear analysis at the Haynes 230 side of the AISI 430/Haynes 230 clad sample after oxidation in coal syngas for 500 hours ..... 59

## ACKNOWLEDGMENTS

I would first like to thank Dr. Scott Mao for his guidance and financial support. Dr. Mao's passion for science has impressed me throughout my study under his direction. My thanks also go to Dr. Mingjian Hua, Cole Van Ormer, Albert Stewart for their help, training and technical support. Special thanks go to Professor Kejia Liu, he was once a visiting scholar in our group and I partially worked with him on this research. I have included the results of some experiment he did on the short-term (100 hours) treated samples in this thesis. I am also grateful to the other faculties and staffs in the Department of Mechanical Engineering and Materials Science, especially Glinda Harvey, for their assistance.

I own acknowledgment to my friends Junhang Luo, Jiazhao Cai, Hao Wang, Dr. Zhenyu Liu, Dr. Guiying Li, Dr. Shaogang Lv and Dr. Jichuan Zhang for their encouragement and help.

Last but not least, I would like to thank the committee members for their time and efforts to improve the thesis.

## 1.0 INTRODUCTION

Solid oxide fuel cell (SOFC) is a promising pollution-free technology to electrochemically generate electricity [1-3]. When compared to other types of fuel cells, SOFCs exhibit low CO<sub>2</sub> emission, fuel flexibility, and high efficiencies. The major issues of SOFCs which need to be resolved are cost-effective manufacturing and long term stability/reliability of the stacks [4, 5]. Among these factors, whether the high cost can be reduced mainly affects SOFCs' future commercial success. In order to minimize the cost, inexpensive, easy-manufacturing stainless steels have been extensively investigated to replace ceramic LaCrO<sub>3</sub> as interconnect materials. So far, only chromia-forming alloys can primarily fulfill most requirements of interconnects.

Currently, a concept of planar SOFCs which use inexpensive coal syngas as the fuel has been proposed. Since the compositions of coal syngas are quite complicated, the oxidation behavior of materials in it should be different from that in hydrogen, which is the conventional fuel used in most fuel cells. Although extensive research has been done to examine the oxidation behaviors of many potential interconnect materials in air, hydrogen and dual-atmosphere, little information about the oxidation properties of these materials in a coal syngas environment are available.

In the present work, the oxidation properties of Fe-based ferritic alloys Crofer 22 APU, E-Brite, AISI 430 and a Ni-based alloy Haynes 230 isothermally exposed in coal syngas at 800 °C for 100 hours and 500 hours were studied. We also tried to develop a continuous oxide scale on

the surface of the materials, exposing the samples in air at 800 °C for 24 hours before put them in a coal syngas atmosphere. The effect of this pre-formed oxide scale on the further oxidation of the alloys in coal syngas was checked with Crofer 22 APU and Haynes 230. Furthermore, the oxidation behaviors of AISI 430/Haynes and E-Brite/Haynes 2300 clad materials were also studied.

## **2.0 BACKGROUND**

### **2.1 FUEL CELL**

Fuel cells have attracted extreme interest as a promising technology for clean power generation. They are electrochemical devices that continuously convert the chemical energy in a fuel (such as hydrogen, natural gas or other hydrocarbon-based fuels) directly into electricity [6]. The basic operating principle of fuel cells was discovered by Christian Friedrich Schönbein in 1838. Based on Schönbein's principle, William Grove developed the first fuel cell in 1939, using a dilute sulfuric acid electrolyte, a hydrogen anode and an oxygen cathode [7]. Fuel Cells have attracted extensive attention after they were successfully used in the US space program in 1960s [8]. Nowadays many different types of fuel cells have been developed and some of them have already been used in a broad spectrum from portable devices, small power systems to spacecraft.

#### **2.1.1 Components and operating principle**

Despite the broad range of different types of fuel cells, the primary components and the working principle are almost the same for all of the fuel cells. A fuel cell comprises of an ion conducting electrolyte, a cathode and an anode. Figure 2.1 is a schematic representation of a fuel cell. A fuel such as hydrogen enters the fuel cell at the anode and an oxidant, typically oxygen, at the cathode. Due to the chemical driving force, at the anode, the hydrogen is oxidized into

protons and electrons, while at the cathode, the oxygen is reduced to oxide species. The electrolyte serves as a barrier to gas diffusion, but will let appropriate ions pass between the anode and cathode. The flow of ionic charge through the electrolyte must be balanced by the flow of electronic charge through an outside circuit, and consequently generates electrical power [6, 9, 10].

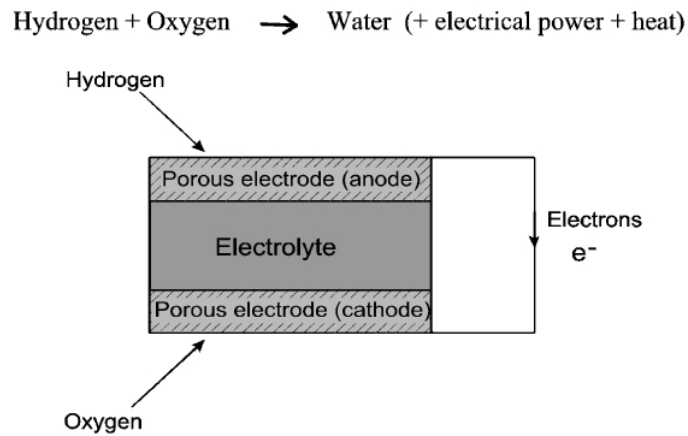


**Figure 2.1:** Schematic illustration of the operating principles of a fuel cell [9]

### 2.1.2 Types of fuel cells

At present, there are five main types of fuel cells based on different electrolyte. They are the polymer electrolyte fuel cell (PEFC), the phosphoric acid fuel cell (PAFC), the molten carbonate fuel cell (MCFC), the alkaline fuel cell (AFC) and the solid oxide fuel cell (SOFC). The main characteristics of these fuel cells are summarized in Table 2. 1.

Although AFC is the oldest fuel cell and it provides extremely high power density, it is considered to be impractical because of the need to remove trace  $\text{CO}_2$  from both the fuel and oxidant streams in order to prevent reaction of the electrolyte to form solid, non-conducting

alkali carbonates. What is more, the strong alkaline solution presents a number of problems. PAFC is the most advance fuel cell at the present stage. The high manufacture cost, however, prevents its commercialization. PEFC has recently attracted significant attention as a potential source of primary power in transportation application and worldwide investment in PEFC continues to grow. Given their high temperatures of operation, MCFC has great applicability in stationary power generation. But it suffers from the difficulties of containing a corrosive liquid electrolyte. In particular, dissolution of NiO at the cathode and its precipitation in the form of Ni at the anode can result in electrical shorts across the electrolyte [8-10]. Although in public eyes, SOFC is not as prominent as PEMFC, it has many advantages such as multi-fuel capability and simplicity of system design. Moreover, the exhaust heat can be used as a heat source for a variety of processes [8].

**Table 2.1:** The main characteristics of different types of fuel cells

	<b>A FC</b>	<b>PEFC</b>	<b>PAFC</b>	<b>MCF C</b>	<b>SOFC</b>
<b>Temperature (°C)</b>	60-120	70-80	220	650-750	800-1000
<b>Electrolyte</b>	KOH	Solid Polymer	Phosphoric acid	Lithium	Solid oxide
<b>Fuel</b>	Pure H <sub>2</sub>	H <sub>2</sub>	H <sub>2</sub>	H <sub>2</sub> , CO, CH <sub>4</sub>	H <sub>2</sub> , CO, hydrocarbons
<b>Efficiency (%)</b>	35-55	30-40	40	>50	>50
<b>Max power (kW)</b>	5	250	200	1000	1000

As mentioned above, the electrolyte of a fuel cell used determines its type. Moreover, it also determines the operating temperature of the fuel cell. The operating temperature is one of the characteristic features of a fuel cell and it, to some extent, determines the application of the fuel cell.

### 2.1.3 Advantages and applications

Fuel cells have many significant advantages over conventional electric power generations. The difference between fuel cells and batteries, the most general electric power generation devices, is obvious. Batteries have all of their chemicals stored inside. When the chemicals are consumed away, the batteries will be “dead”. While for fuel cells, the electrodes are catalytic and relatively stable. This means that as long as there is a flow of chemicals into the fuel cell, the electricity flows.

Fuel cells are fascinating for the high energy conversion efficiency and extremely low emission of pollutants. Because there is no direct combustion in a fuel cell system and the byproduct is  $H_2O$ , the application of fuel cells brings no pollution and consequently reduces the environmental pressure. This makes fuel cells attractive for transport application, especially in big cities. Developing fuel cell powered cars and buses is currently an field of intense activity for motor manufactures.

Stationary power generation is viewed as the broadest market for fuel cell. The reduction of  $CO_2$  emission is an important argument for the use of fuel cells in stationary power systems [7]. Unlike conventional stationary power systems which use combustion technologies, fuel cell systems can be built in a wide range of sizes: from 200 kW units suitable for powering commercial buildings to 100 MW plants [12].

Moreover, a fuel cell system can be compact, light weight and has no major moving parts. It can serve as power sources in remote locations, such as spacecraft, remote weather stations and some military application [11]. These years, there is a rapid increase of applications of fuel cell in cell phone, lap-top and other small portable devices which require just few watts.

The biggest disadvantage of fuel cells is the high manufacture cost. In order to be competitive, fuel cells must cost below \$35 per kilowatt [13]. However, the current price is much higher than this. Another serious problem is no good ways for on-site desulfurization of hydrocarbon fuels and this presents a challenge for using hydrocarbon fuels [12]. Other challenges fuel cell developers are facing include improving the durability, lowering the operating temperature, and developing cheaper materials for each component.

## 2.2 SOLID OXIDE FUEL CELLS (SOFCs)

### 2.2.1 Operating principle

The characteristic feature that distinguishes SOFCs from other types of fuel cells is the solid electrolyte. The dense electrolyte is sandwiched between the anode and cathode. The operating principle and basic components for SOFCs are the same as other fuel cells, as mentioned above. The electrode reactions for SOFCs are: given below.

At the cathode, oxygen is reduced via:



$\text{O}^{2-}$  migrates from the cathode to the anode through the dense electrolyte.

At the anode,  $\text{O}^{2-}$  reacts with hydrogen or CO, producing  $\text{H}_2\text{O}$  and/or  $\text{CO}_2$ :



Therefore, electrons are released at the anode and migrate from the cathode through an external electric circuit, thus producing an electric current. At the same time, water is produced at the anode as byproduct. The overall reaction can be written as:



### 2.2.2 Design of SOFCs

SOFCs have been made into various shapes: tubular, flat plate, bell-and-spigot, banded, and corrugated [15]. Each shape results in distinct current paths and different cell configurations. The configurations in SOFC include: electrolyte-supported, cathode-supported, anode-supported, porous substrate-supported and interconnect-supported [14].

Actually, all the challenging aspects of SOFCs design and manufacture are material-related. SOFCs place severe demands on the materials used as the components, namely, the electrolyte, anode, cathode and interconnect. Each component must meet certain critical requirement. All components must possess chemical and physical stability in an appropriate chemical environment, be chemically compatible with the other components, have proper conductivity, and have similar thermal expansion coefficients to the other components to avoid fracture due to thermal effects. Although many kinds of materials have been developed for SOFCs, at the current stage, almost all SOFCs use an yttria-stabilized zirconia electrolyte, a strontium-doped lanthanum manganite ( $\text{La}_{1-x}\text{Sr}_x\text{MnO}_3$ ) cathode, a mixed nickel/yttria-stabilised zirconia (YSZ) cermet anode, and doped lanthanum chromite ( $\text{LaCrO}_3$ ) or metallic interconnects [9].

### **2.2.3 Advantages**

The primary advantage of SOFCs over other fuel cells is that SOFCs can use a wider range of fuels, such as hydrocarbons. The flexibility in fuel choice makes SOFCs particularly suited to small-scale and remote application. Besides, the efficiency is considerably higher than any other fuel cells and can be up to 65%. Furthermore, due to their high operating temperature, typically in the range of 800-1000°C, hydrocarbon fuels such as methane and natural gas can be reformed within the stack, eliminating the need of an expensive external reformer system [16]. Lastly, the system design of SOFCs is simple and cheap conventional ceramic manufacturing processes can be used to develop large SOFCs.

Although SOFCs have many advantages and potential applications, the disadvantages are obvious. The main issues that affect the commercialization of SOFC are the short life time and the high cost. Moreover, due to the high operating temperature, the relative long start-up and cool down period limit the application of SOFCs to stationary and auxiliary power units.

## **2.3 INTERCONNECTS OF SOFCs**

### **2.3.1 The roles of interconnects**

The interconnect is one of the four main components of a fuel cell. Its critical role is to provide electrical connection between the anode of one cell to the cathode of the neighbor one and therefore to form a stack. It also acts as a physical barrier to protect the air electrode material from the reducing environment of the fuel on the fuel electrode side. At the same time, it

prevents the fuel electrode material from contacting with oxidizing atmosphere of the oxidant electrode side [17]. Moreover, in some cases, it acts as the primary structural element to maintain the overall mechanical support (for example, in SOFCs of interconnect-supported configuration) and stability of the stack.

### **2.3.2 The requirements**

The requirements for interconnects of SOFCs are quite stringent. To effectively perform their functions, interconnects need to fulfil the following conditions, which are summarized by Zhu and Deevi in reference (17).

1. Interconnects must exhibit excellent electrical conductivity.
2. Interconnects should have adequate stability in terms of dimension, microstructure, chemistry and phase at the high operating temperature of about 800-1000°C.
3. The thermal expansion coefficient of interconnect should be comparable to other components in a SOFCs.
4. Interconnects should display exceptionally low permeability for oxygen and hydrogen to minimize the direct combination of oxidant and fuel during cell operation.
5. They has no reaction or inter diffusion between interconnect and other components.
6. They should have good thermal conductivity.
7. Interconnects should have excellent oxidation, sulfidation and carburization resistances.
8. In some cases, they should have adequate high temperature strength and creep resistance.

### 2.3.3 The materials for interconnects

Two main types of materials have been developed for interconnects of SOFCs: ceramic and metallic alloys.

The extensively accepted ceramic interconnects are primarily doped lanthanum and yttrium chromites ( $\text{LaCrO}_3$ ). The presence of dopants ensures chemical stability and thermo-mechanical characteristics [6]. This kind of ceramics show high electrical conductivity and high corrosion resistance in an oxidizing atmosphere as well as in a reducing atmosphere. The two main drawbacks of ceramic interconnects are high cost and brittleness [17].

When the operating temperature of SOFCs is in the range of 600-800 °C, appropriate metallic alloys can be used to replace ceramic as alternative interconnect materials. In general, metallic interconnects have many advantages over ceramic ones: higher electronic and thermal conductivity, low cost, easy manufacture and good workability.

Because the surfaces of interconnects are exposed in high temperature oxidation atmosphere, an oxide layer will inevitably form for metallic interconnects. To keep the high efficiency and structural stability of the fuel cell, the oxide scale needs to have sufficiently high electronic and thermal conductivity, chemical stability, good adhesion with the substrate and low grow-rate.

Although at high temperatures, the oxidation resistance of  $\text{Al}_2\text{O}_3$ - and  $\text{SiO}_2$ - forming alloys is generally better than other alloys [18], they cannot be used as interconnects due to the electrically-insulating nature of the alumina and silica scales. At the current stage, only chromia-forming alloys are selected as SOFC interconnects and they can primarily fulfil most requirements listed above.

When chromia-forming alloys are used as interconnects, chromia scales grow by outward diffusion of chromium ions, which results in the formation of porosity at the alloy-scale interface, and when combined with significant growth stresses, can lead to scale cracking and spallation [19]. Another serious problem is that the migration of the Cr species in SOFCs can poison the cathode, leading to the performance degradation of SOFC stacks over long term operation (up to 40,000 hours) [20]. All kinds of chromia-forming alloys have to face these problems.

The chromia-forming alloys that have been used as interconnect include Cr-, Fe-, and Ni-based alloy. We will briefly discuss them in the following part, separately. The detailed reviews of interconnect materials for SOFCs by Zhu et al can be found in reference (16, 17).

### **Chromium-based alloys**

Chromium-based alloys are acceptable interconnect materials due to their moderate oxidation resistance and good corrosion resistance provided by the formation of  $\text{Cr}_2\text{O}_3$  chromia scales. Moreover,  $\text{Cr}_2\text{O}_3$  scales have good electronic conductivity and the thermal expansion behaviors are very similar with  $\text{LaCrO}_3$  in the temperature range of 25 to 1000°C [21].

The main drawback of this type alloys is the high oxidation rate, which is usually four orders higher than that of Al-based alloys at high temperatures. Trace amounts of reactive element such as Y, La and Ce are usually added to the basic alloys to improve the oxidation resistance. Thus, some special alloys, such as Cr-5Fe-1.3La<sub>2</sub>O<sub>3</sub>, Cr-5Fe-0.5CeO<sub>2</sub> and Cr-5Fe-0.3Ti-Y<sub>2</sub>O<sub>3</sub>, have been developed for SOFC interconnect applications. These reactive elements can not only improve the oxidation resistance by retarding the kinetics of the scaling process, but

also refine the grain size of the oxide layer via the dragging mechanism [16, 21]. In addition, the integrity of the scale can be substantially strengthened owing to the greatly suppressed scale spallation tendency.

Another problem of chromium-based alloys is the formation of volatile gaseous Cr (VI) species at high temperatures. These high valence species such as  $\text{CrO}_3$  and  $\text{Cr}(\text{OH})_2$  form with  $\text{Cr}_2\text{O}_3$  scale at the cathode side and diffuse into and interact with some kinds of air electrodes, leading to a change of the electrode composition and deposit  $\text{Cr}_2\text{O}_3$  on the electrode/electrolyte interface [16], which is damageable to fuel cells. Some special coatings such as lanthanum strontium-doped-manganite or cobaltite are used to mitigate the Cr volatilization effects [22].

### **Iron-based alloys**

Iron-based alloys have apparent advantages over chromium-based ones. In general, they have high ductility, good workability and low cost. Usually, the iron-based alloys for interconnect use at least contain 17 wt% Cr to form corrosion-resistant  $\text{Cr}_2\text{O}_3$  scale. These alloys include: Fe-10Cr, Fe-26Cr-1Mo, Fe-16Cr-0.2Y, Fe-17Cr-0.5Y-2Ni, and Fe-26Cr-Mo-Ti-Y etc. For Fe-Cr alloys containing neither reactive nor alloying element, the growth rate of the oxide scale is exceedingly high, making these alloys unacceptable for interconnect use.

As chromium-based alloys, addition of small amounts of reactive and alloying elements is beneficial for iron-based alloys because they can improve the scale adherence and decrease the scale growth rate. It has been found that addition of Mo can moderately suppress the growth kinetics of  $\text{Cr}_2\text{O}_3$ . Researchers also found that Mn can be added to develop spinel ( $\text{Cr}_2\text{MnO}_4$ ) scale on the top of  $\text{Cr}_2\text{O}_3$  scale. Thus, although the total scale thickness increases, the electrical

resistance can be greatly decreased due to the relatively low electrical resistivity of Cr/spinel phase [17].

### **Nickel-based alloys**

Nickel and Nickel-based alloys have also been investigated for interconnect use. Well-studied alloys include Haynes 230, Inconel 625, Inconel 718, and Inconel 600. They usually contain Ni, Cr, Fe and Mn. These alloys are attractive for SOFC interconnect application due to their slower oxidation kinetics. However, the large thermal expansion coefficients to some extent limit their application as interconnect, because the mismatch thermal expansion will cause high thermal stresses between the components and form cracks. To overcome this disadvantage, elements such as molybdenum and tungsten can be added to get a better match of the thermal expansion coefficient between the oxide scale and the substrate. Moreover, interconnects of Ni-based alloys are usually made in foil of about 0.1 mm thick to solve the thermal expansion match problem.

## **2.4 INTRODUCTION OF HIGH-TEMPERATURE OXIDATION**

Almost all metallic materials are subject to deterioration in air or where oxygen exists. Deterioration at low temperatures is usually referred as corrosion and at high temperatures it is called oxidation. The nature of corrosion and oxidation is the same, i. e., metals reaction with oxygen to form an oxide layer on the surfaces.



In general, the oxidation rate increases rapidly with the temperature due to the large diffusion coefficient of oxygen at high temperatures. Therefore, only specially selected alloys can be used at high temperatures. High-temperature oxidation is an extensively investigated subject of material engineering. In this section, we will briefly introduce the basic thermodynamic and mechanisms of high-temperature oxidation of metals and alloys. This is summarized from reference (23).

### 2.4.1 Thermodynamics

Gibbs free energy ( $G'$ ) of a system is usually used to determine whether oxidation can occur or not.

For a chemical reaction:



the change of Gibbs free energy ( $\Delta G^0$ ) at equilibrium state can be expressed by:

$$\Delta G^0 = -RT \ln K_{eq} \quad (2.6)$$

where  $K_{eq}$  is the reaction equilibrium constant, which represents:

$$K_{eq} = \frac{a_C^c a_D^d}{a_A^a a_B^b} \quad (2.7)$$

where  $a_i$  is the thermodynamic activity of  $i$  species. It is a dimensionless number and expressed by:

$$a_i = \frac{P_i}{P_i^0} \quad (2.8)$$

where  $p_i$  is the vapor pressure over a condensed species, or the partial pressure of a gaseous species and  $p_i^0$  is the same quantity corresponding to the standard state of  $i$ .

Plots of standard free energy of oxide formation versus temperature, commonly known as Ellingham diagrams, can be used to compare the relative stabilities of oxides under a particular environment. Figure 1.2 is an Ellingham diagram of some simple oxides. One can use it to determine which reaction products are possible, whether or not significant evaporation or condensation of a given species is possible, and the conditions under which a given reaction product can react with a condensed deposit, etc.

#### **2.4.2 Mechanism of oxidation**

Initially, oxidation occurs by a series of reactions involving the adsorption and dissociation of the oxygen molecules in the gas, leading to the incorporation into the metal lattice. Oxide nuclei then form and grow [24]. The adsorption and initial oxide formation are functions of the metal surface and impurities in both the metal and gas [25].

After a continuous oxide layer is formed, to keep the oxidation process to continue, one or both reactants (metal and oxygen) must penetrate the oxide scale to react with each other. Clearly, this is a diffusion process and is controlled by the diffusion coefficients of the atoms. This transport of oxygen anions or metal cations is driven by a chemical potential gradient that is created across the scale. The ions transport across the oxide layer as shown in Figure 2.3. The activities and partial pressures at both interfaces are fixed by thermodynamic equilibrium. At the interface of the metal and oxide, the oxygen pressure in the ambient atmosphere is used to calculate the activity of the metal in the oxide layer.

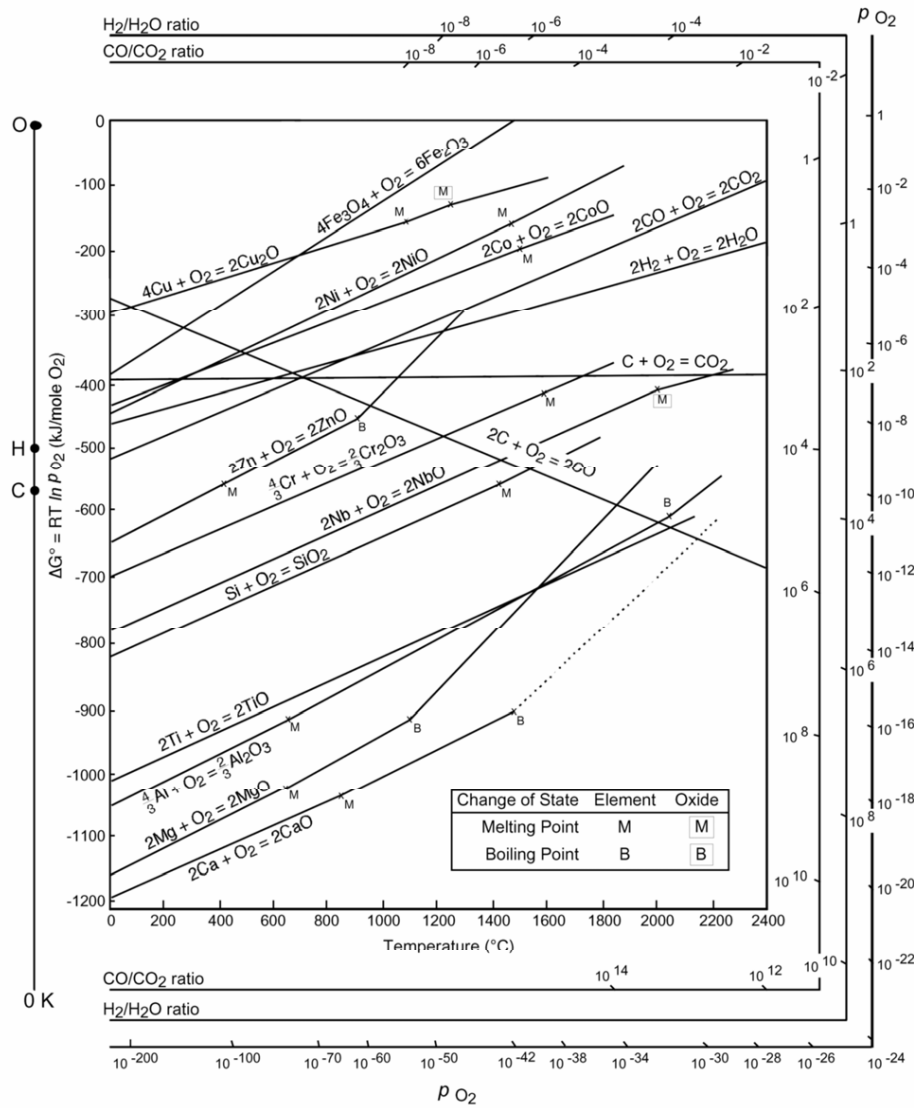
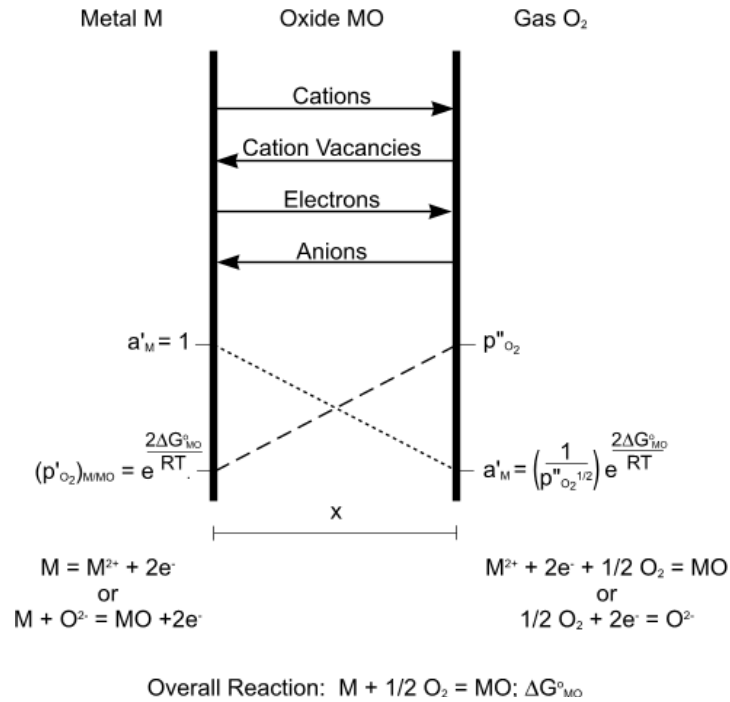


Figure 2.2: Ellingham diagram of some selected simple oxides. [23]

As the oxide layer thickness increases, the diffusion distance of ions consequently increases, leading to a decreasing growth rate of the oxide layer. Wagner [23] found that under some conditions, the growth of the oxide could be characterized by a parabolic equation:

$$X^2 = 2k_p t \quad (2.9)$$

where X is the oxide thickness,  $k_p$  is the parabolic rate constant and t is the time.



**Figure 2.3:** Schematic diagram of the mechanism of oxidation [23]

### 2.4.3 Oxidation of alloys

Although the general principle is the same, oxidation of alloys is much more complicated than that of pure metals. This is due to some of the reasons or their combination listed below [23, 25].

1. Each element in an alloy has different chemical properties and the reaction with oxygen is different;
2. A degree of solid solubility may exist between the oxides;
3. Dissolution of oxygen into the alloy may result in sub-surface precipitation of oxides with different alloying elements.

4. The oxide may grow and consume one of the metals over the others and consequently concentration gradient of this element may exist in the alloy.

Oxidation of alloys can be classified into two groups: (1) noble parent with base alloying elements and (2) base parent with base alloying elements [23]. The first group includes alloying elements, such as Au, Ag, Pt etc., which cannot form stable oxide under normal conditions with alloying elements such as Cu, Ni, Fe, Co, Al, Ti, etc., which form stable oxides. At reduced oxygen partial pressure, these elements such as Cu, Ni can act as noble-parent metals in the alloys.

The second group of alloys consists of a base of stable oxide forming element, such as Ni, Fe, and Co, and an alloying element such as Cr, Al and Si, which forms a highly stable oxide. This kind of alloys represents most of commercially available alloys, such as Ni-Cr, Fe-Cr and Co-Cr alloys.

#### **2.4.4 Oxidation of interconnects**

Interconnects are exposed to air at the cathode and to a reducing atmosphere at the anode. At high temperatures, there is a large oxygen partial pressure gradient. In such a condition, a gradient of chemical potential gradient is also set up for each element of the alloy and causes oxidation. Oxidation of interconnect may form oxide scales, increase electronic (area specific) resistance, and destroy the electrodes.

As for the oxidation rate, chromia-forming alloys typically do not follow a simple parabolic rate law as represented by equation 2.9. At high temperatures, oxidation follows a parabolic relationship due to a volatilization of the chromia scale. Figure 2.4, for example, is the plot of the

square of the weight change, which represents the oxidation rate, versus time for a Ni-based alloy. We can see the oxidation rate decreases significantly over time at high temperatures.

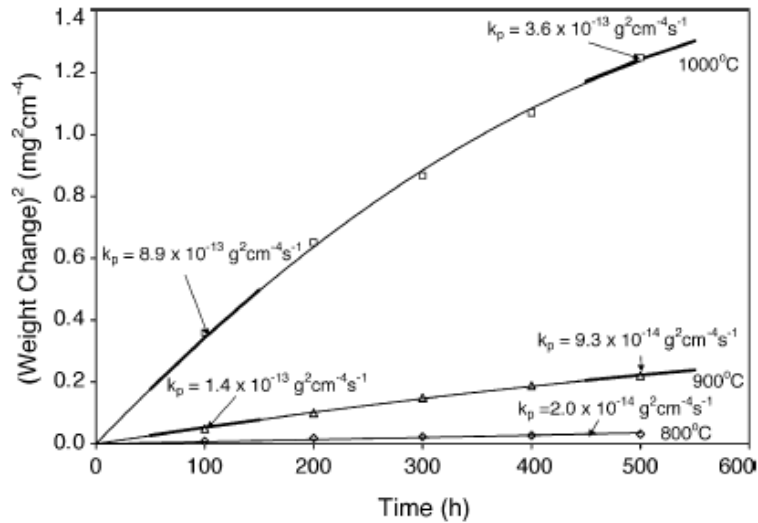
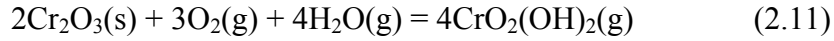
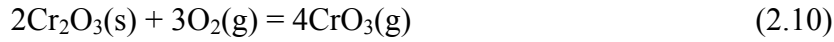


**Figure 2.4:** Weight change of ASL 528 during oxidation in air at 800-1000 °C [19]

For most SOFCs, hydrocarbon is used as fuels. A main problem for metallic interconnects working at a carbon-containing atmosphere is the formation of carbides or graphite [19]. The most likely location for the occurrence of carbides is near the inlet of the carbon-containing fuel (e.g. methane), where the reactant (methane) concentration is the highest and the product (water vapor) concentration is the lowest. The first step in carbide formation is the dissolution of carbon into the metal, so austenitic stainless steels, due to their higher solubility and diffusivity of carbon, are more susceptible than ferritic stainless steels. However, ferritic, rather than austenitic, stainless steels are used for SOFC interconnects, so this is not a significant problem.

Another serious problem for metallic interconnect, as mentioned in section 2.3.3, is Cr oxide vaporization and deposition. Under cathodic conditions, volatile Cr (VI) species in the

form of either  $\text{CrO}_3(\text{g})$  or  $\text{CrO}_2(\text{OH})_2(\text{g})$  is generated simultaneously with the  $\text{Cr}_2\text{O}_3$  layer via the following reactions:



The electrochemical performance of SOFCs is seriously damaged due to the presence of gaseous chromium oxides and chromium oxyhydroxides at the cathode side of the fuel cell. The reduction of volatile Cr (VI) species to solid  $\text{Cr}_2\text{O}_3$  is deemed to be responsible for the property degradation [17, 19].

Studies also found that small amount of  $\text{H}_2\text{O}(\text{g})$  could significantly increase Cr oxide vaporization because the formation of  $\text{CrO}_2(\text{OH})_2(\text{g})$  is favored from the standpoint of vapor pressure. This is especially harmful for SOFCs since the fuel gases invariably involve some  $\text{H}_2\text{O}$  and it is the main byproduct of reactions [17].

#### **2.4.5 Protection of interconnects**

Coatings have been widely used to protect the substrate materials. Many different coatings have been developed for SOFC interconnects with different purposes. For chromia-forming alloys used as interconnects, the coatings are mainly intended to prevent chromium vaporization and migration [26]. It was found that a coating such as  $(\text{La,Sr})\text{CrO}_3$  or  $(\text{La,Sr})\text{MnO}_3$  could significantly reduce the amount of chromium vaporization. By coating a chromium-based alloy with  $\text{La}_{0.9}\text{Sr}_{0.1}\text{CrO}_3$ , the chromium vaporization rate was decreased by a factor greater than 100 [27]. Currently, Mn-containing coatings have attracted attention. The ferritic stainless steel, Crofer 22 APU, was specially developed to form a spinel  $(\text{Cr, Mn})_3\text{O}_4$  layer to protect Cr migration. It was

reported a sintered spinel  $(\text{Mn,Co})_3\text{O}_4$  layer developed on Crofer 22 APU not only significantly reduced the interfacial area specific resistance (ASR) and the growth rate of the scale, but also drastically prevent Cr migration [28]. Spinel  $\text{MnCo}_2\text{O}_4$ , and  $\text{Cu}_{1.4}\text{Mn}_{1.6}\text{O}_4$  can also inhibit Cr migration and show good structural and thermal stability at high temperature.

Another way to optimize interconnect materials is so called cladding. Since few metallic alloys can completely fulfil the requirement for SOFC interconnects, people try to bond different alloys with different compositions and properties together to form a double- or multi-layer material, integrating the advantages of these different alloys while avoiding their disadvantage [29, 30]. Chen et al. [29] demonstrated that this would be a promising method for SOFC interconnect manufacture. Two typical types of cladding can be used for SOFC interconnects. The first one is simply bonding two or more layers of metals with different properties together. For example, a ferritic stainless steel with an appropriate level of Cr and low thermal expansion coefficient can be used as the base materials, and a relative high thermal expansion coefficient austenitic high temperature oxidation resistant alloy is used to form a thin surface layer on the base alloy. The ferritic stainless steel lowers the cost while the surface layer alloy provides acceptable thermal stability. The second one is that first bonding different alloys together and then modifying the clad materials by heat treatment. During the heat treatment process, diffusion occurs at the interface of the different layers and finally forms a special layer which may be different from the original components of the clad materials. This method can be used to modify and optimize the interconnect materials to get the well-designed properties.

### **3.0 MOTIVATION AND OBJECTIVE OF THE STUDY**

As briefly discussed in Chapter 2, appropriate chromia-forming alloys can be used to replace ceramic as SOFC interconnects. Some Cr-, Fe-, and Ni-based alloys have been developed for this application. Nowadays industries and researchers are interested in developing planar SOFCs which use inexpensive coal syngas as the fuel. Coal syngas typically consists of CO and H<sub>2</sub> and other compositions such as CO<sub>2</sub>, H<sub>2</sub>O, N<sub>2</sub>, CH<sub>4</sub> and H<sub>2</sub>S. Long time exposure to a coal syngas environment at a high temperature of 800-1000 °C will cause the degradation of the metallic interconnects. Although extensive research have been done to examine the oxidation behaviors of many potential interconnect materials in air, hydrogen and dual-atmosphere, little information of the oxidation properties of these materials in a coal syngas environment are available.

In the present work, the oxidation behaviors of several potential interconnect materials in a high temperature coal syngas environment were evaluated. The effect and feasibility of pre-oxidation and cladding on the oxidation resistance of these materials were investigated.

## 4.0 EXPERIMENTAL PROCEDURES

### 4.1 MATERIALS

The materials used in this study are those which are regarded as the most promising potential interconnect alloys, including Crofer 22 APU, Ebrite, Haynes 230 and AISI 430. The composition of these alloys are listed in Table 4.1.

**Table 4.1:** Composition (in wt.%) of the selected alloys

	Cr	Fe	Ni	C	Mn	Si	Al	Ti	Cu	Others
Crofer 22	24	73.2	—	.03	.8	.50	.50	.2	.50	S .02, P 0.05, La .2
E-Brite	26.3	71.86	0.15	—	.1	.21	.05	.05	.05	Mo 1.01, P .01, Cd .12
Haynes 230	22	3	52.7	.1	.5	.4	.3			Co 5, W 14, Mo 2, B .15
AISI 430	17	81.6	.18	.1	.5	.51			.04	N .02, Mo .01, P 0.04

#### 4.1.1 Crofer 22 APU

Crofer 22 APU is a high temperature ferritic stainless steel developed by ThyssenKrupp to be specifically used for interconnects in SOFCs. A double-layer oxide with a  $(\text{Cr, Mn})_3\text{O}_4$  spinel outer layer on the top of a  $\text{Cr}_2\text{O}_3$  inner layer formed at a high temperature.  $(\text{Cr, Mn})_3\text{O}_4$  has a high electrical conductivity and is very stable. This protective oxide significantly reduces the evaporation of chromium. Moreover, the low coefficient of thermal expansion is matched to  $\text{LaCrO}_3$ . [31]

#### **4.1.2 E-Brite**

E-Brite, produced by Allegheny Ludlum, is another ferritic stainless steel as a potential SOFC interconnect material. This alloy is essentially a Fe-26Cr alloy. It has a high chromium content that can form a protective oxide layer on the surface. Moreover, the spallation of the protective oxide layer is prevented due to its low thermal expansion coefficient. In addition, compared to conventional ferritic stainless steels, E-Brite has an improved ductility and formability due to additions of carbon and nitrogen [32].

#### **4.1.3 Haynes 230**

Haynes 230, from Haynes International, is a Ni-based austenitic alloy. The biggest advantage of Haynes 230 is its high resistance to high temperature warpage and oxidation. It can stand long-term continuous exposure at temperatures as high as 1149 °C. The resistance to oxidation, combustion environments and nitriding makes it suitable for applications such as nitric acid catalyst grids, high-temperature bellows, industrial furnace fixtures and thermocouple protection tubes [33]. Haynes 230 is less popular than ferritic alloys for SOFC interconnects due to the high thermal expansion coefficient which does not well match that of other components of SOFCs, but the thermal expansion coefficient is still acceptable. It was found that after oxidation in air and wet hydrogen at a temperature between 700 and 1000 °C for up to 10000 hours, the area-specific resistance of Haynes 230 was still suitable for interconnect applications [34, 35].

#### 4.1.4 AISI 430

AISI 430 is a ferritic, non hardenable stainless steel, combining good corrosion resistance and formability. It has good resistance to a wide variety of corrosive media, including nitric acid, which makes it suitable for specific chemical application. AISI430 is typically used as automotive and architectural trim, vaults, heat exchangers, scientific apparatus and vending machine components.

## 4.2 MATERIALS PREPARATION

Rectangular samples of 10×10×(1-2) mm in size were cut from the sheets of each alloy. The samples were ground up to 800 grits with SiC sand paper, ultrasonically cleaned in acetone, and then dried before the oxidation treatment.

Oxidation was isothermally conducted in a horizontal furnace. Specimens were put in an alumina boat and exposed to a flowing carburizing atmosphere at 800°C. The coal syngas was the simulation of a reformer outlet one, and the compositions were (in vol.%) 29.1CO + 28.5H<sub>2</sub> + 11.8CO<sub>2</sub> + 27.6H<sub>2</sub>O + 2.1N<sub>2</sub> + 0.01CH<sub>4</sub>, and also contained 100 ppm H<sub>2</sub>S.

The samples were exposed in coal syngas for 100 hours and 500 hours to compare their short-term and long-term oxidation properties. Some Crofer 22 APU and Haynes 230 samples were first isothermally exposed in air for 24 hours to develop a continuous oxide scale, and then they were further oxidized in coal syngas for 500 hours to study the effect of the pre-formed oxide scales on the oxidization behavior of the alloys. The clad materials of E-Brite/Haynes 230 and AISI 430/Haynes 230 were also exposed in coal syngas at 800 °C for 500 hours.

### **4.3 CHARACTERIZATION**

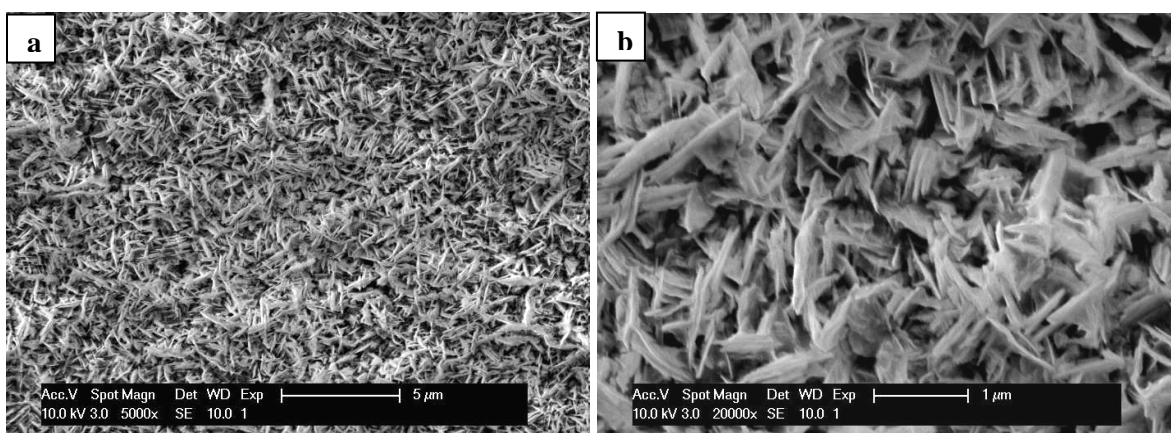
XRD analysis was conducted on a Philips X'pert diffractometer. The scan range was from 20 degrees to 80 degrees. A Philips XL-30 field emission scanning electron microscope (SEM) was used to study the surface morphology and the cross sectional structure of the oxide scales formed on the alloys, with an accelerating voltage of 10 KV and a spot size of 3. The magnifications used in this experiment were 5000 and 20000 and the mode is secondary electron (SE). The element distribution in the scales was analyzed using an energy-dispersive X-ray spectroscopy (EDX) which is an accessory of the SEM. The accelerating voltage used for EDX analysis was 15 KV and the spot size was 4.

## 5.0 RESULTS AND DISCUSSION

### 5.1 CROFER 22 APU

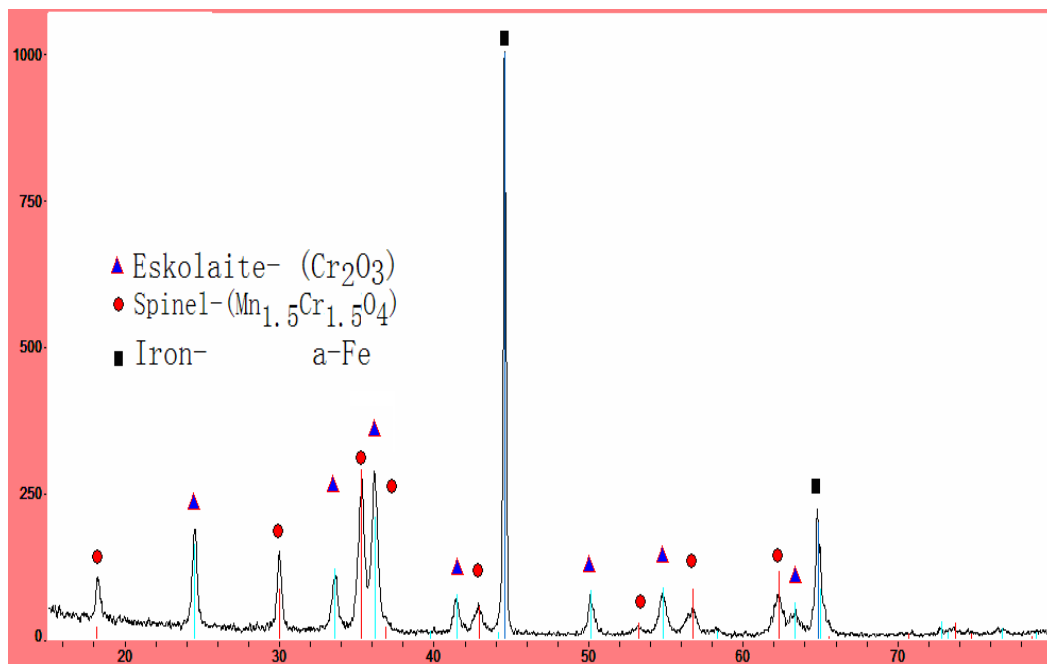
#### 5.1.1 Exposed in coal syngas at 800 °C for 100 hours

Figure 5.1 is the SEM surface morphology of Crofer 22 APU which had been exposed in coal syngas at 800 °C for 100 hours. The surface consisted of uniform whisker-like grains with random orientations. The size of the grains was roughly 1  $\mu\text{m}$  in length and 0.2 $\mu\text{m}$  or less in thickness. These grains were not close-packed and the surface of the sample was porous.



**Figure 5.1:** SEM morphology of the surface of Crofer 22 APU exposed in coal syngas for 100 hours: (a) 5000X, (b) 20000X

EDX point analysis indicated that the grains were rich in Cr (24 Wt%) and Mn (16.5 Wt%) and the main phase should be  $Mn_{1.5}Cr_{1.5}O_4$  spinel. The XRD pattern of the sample's surface, as shown in Figure 5.2, confirmed that  $Mn_{1.5}Cr_{1.5}O_4$  spinel existed in the surface oxide scale. Besides the peaks corresponding to the spinel phase,  $Cr_2O_3$  chromia and the metal substrate peaks also appear in the XRD patterns due to X-ray penetration through the thin scale to the underlying substrate alloy.



**Figure 5.2:** XRD pattern of scales grown on Crofer 22 APU exposed in coal syngas for 100 hours

The SEM cross-sectional microstructure and elemental distributions of the sample are given in Figure 5.3. We can see that the oxide scale had a double-layer structure. The outer thin layer was about  $0.7 \mu m$  thick and rich in Mn. Combined with the EDX point analysis, this layer was determined to be  $Mn_{1.5}Cr_{1.5}O_4$  spinel. The inner layer was about  $2 \mu m$  in thickness and it should be  $Cr_2O_3$ . Some Al-containing phase(s) existed in the spinel layer and at the interface between

the spinel and chromia layer. Although no Si or C phase was detected in the oxide scale, we cannot exclude the possibility that some amorphous Si and/or C phases might exist. Moreover, due to the resolution limit of the EDXS analysis technique, trace amount Si/C-containing phase might not be detected.

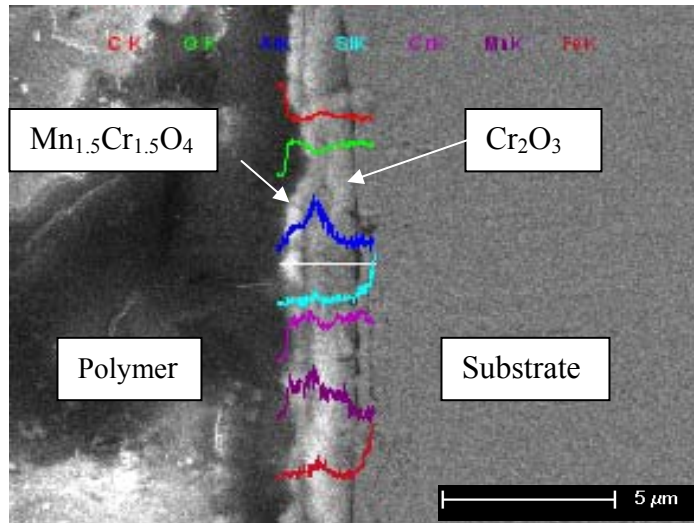


**Figure 5.3:** EDX linear analysis of the cross section of the oxide scale of Crofer 22 APU exposed in coal syngas for 100 hours

### 5.1.2 Exposed in coal syngas at 800 °C for 500 hours

The surface of the Crofer 22APU exposed in coal syngas at 800 °C for 500 hours was quite irregular and porous, as shown in Figure 5.4 (a). A closer look (Figure 5.4 (b)) revealed that the surface consisted of prism-like grains as well as round grains. The prism-like grains are generally larger in size than the other type and it looks like these grains were randomly piled up.

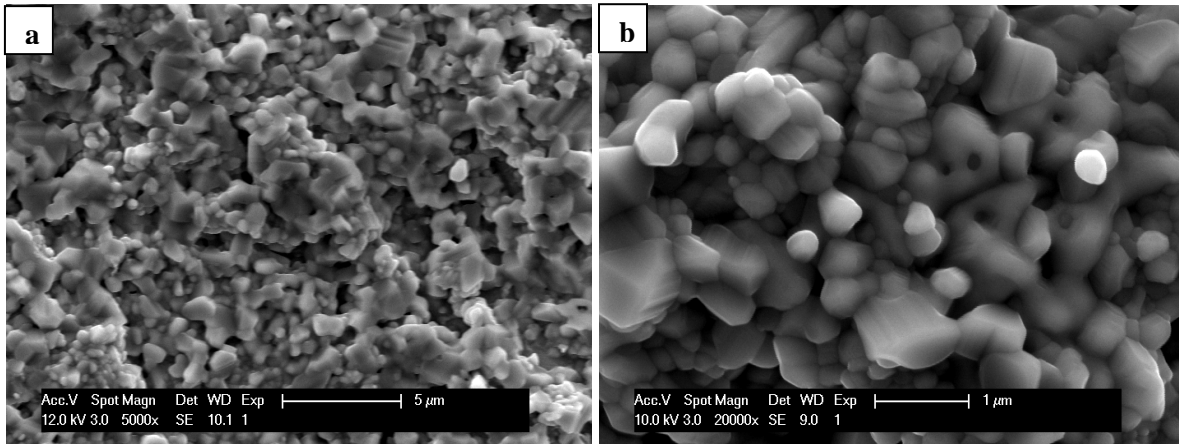


**Figure 5.4:** SEM morphology of the surface of Crofer 22APU exposed in coal syngas for 500 hours: (a) 5000X, (b) 20000X

The XRD analysis revealed that the scale mainly consisted of  $Mn_{1.5}Cr_{1.5}O_4$ ,  $Cr_2O_3$  and  $(Mn,Fe)_2SiO_4$ , see Figure 5.5. The elemental distribution in the oxide scale is shown in Figure 5.6 (a). We can see that the discrimination between the spinel and chromia phase in Figure 5.3 disappeared and the elements of Mn, Cr, Si and O tended to become homogenous through the thickness. This was consistent with the results of Yang et al [36]. They found that in the early stages of the oxidation process of Crofer 22 APU in air at 800 °C, the scale had two layers which mainly consisted of  $Mn_{1.5}Cr_{1.5}O_4$  and  $Cr_2O_3$ , respectively. As the time increased to 300 hours, the scale surface became smoother, the contrast between the spinel and chromia became indiscernible, and the scale composition and microstructure became homogenous.

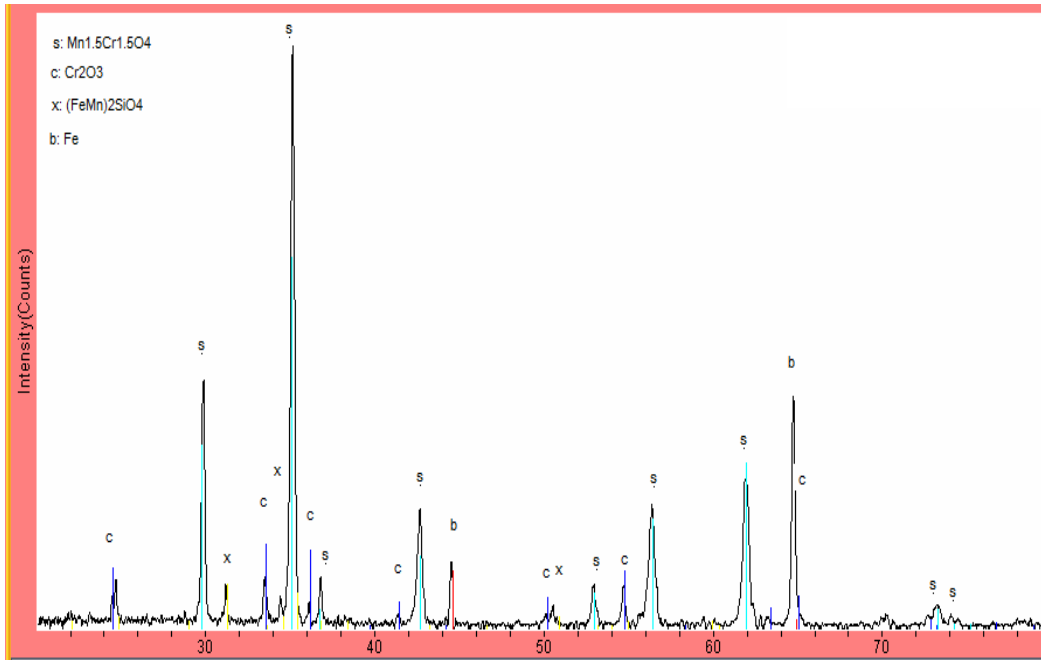


**Figure 5.5:** XRD pattern of scales grown on Crofer 22 sample exposed in coal syngas for 500 hours

It should be noticed that although other elements homogeneously distributed in the scale, C mainly concentrated in the outer layer. It is interesting to see that this C concentrated layer had a different contrast from the inner layer. This can be seen more clearly in Figure 5.6 (b). Although the inner layer and the substrate had a well-bonded interface, it had bad adhesion with the C concentrated layer. This may be due to the presence of carbide precipitates which had a detrimental effect on the adhesion of the scale.

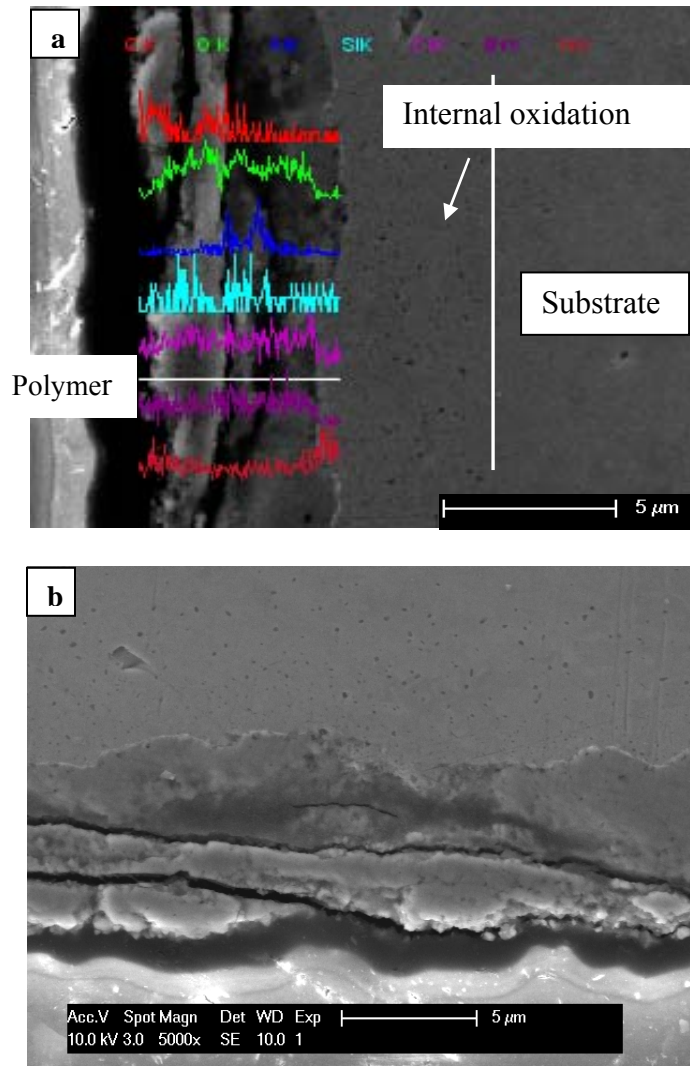


**Figure 5.6:** (a) Cross-sectional EDX linear analysis of the oxide scale of Crofer 22 APU exposed in coal syngas for 500 hours; (b) SEM morphology of the cross section

Many small black spots could be seen on the surface of the substrate alloy. These spots concentrated in a zone with a thickness of 5 μm or so. This zone might be an internal oxidation layer and the black spots may be TiO<sub>2</sub>, aluminum oxide or other oxide. However, this kind of internal oxidation layer cannot be found on the morphology of the sample exposed in coal syngas for 100 hours.

In summary, when compared to the sample exposed in coal syngas for 100 hours, the sample for 500 hours had a  $\text{Mn}_{1.5}\text{Cr}_{1.5}\text{O}_4$  and  $\text{Cr}_2\text{O}_3$  homogeneously-distributed layer.  $(\text{Mn,Fe})_2\text{SiO}_4$  was also detected in the scale after oxidation for 500 hours but not in the sample for 100 hours. XRD and EDX linear analysis revealed that the amount of  $(\text{Mn,Fe})_2\text{SiO}_4$  was small and evenly distributed in the scale. The difference of the surface morphology might be due to that the surface phase of the sample exposed for 100 hours was  $\text{Mn}_{1.5}\text{Cr}_{1.5}\text{O}_4$ , while that of the other sample was the combination of  $\text{Mn}_{1.5}\text{Cr}_{1.5}\text{O}_4$ ,  $\text{Cr}_2\text{O}_3$ ,  $(\text{Mn,Fe})_2\text{SiO}_4$  and some carbides.

### 5.1.3 Pre-oxidized samples

As discussed in Chapter 4, coating has been extensively used for protection of metallic interconnects of SOFCs to achieve satisfactory long-term (40,000 hours) performance. For ferritic stainless steels, one of the most effective coatings is  $\text{Mn}_{1.5}\text{Cr}_{1.5}\text{O}_4$ . It has been found that  $\text{Mn}_{1.5}\text{Cr}_{1.5}\text{O}_4$  spinel protective coating could significantly reduce oxide scale growth kinetics and Cr volatility and demonstrated long term structural, thermo-mechanical, and electrical stability [37, 38].

In the present work, Crofer 22 APU and Haynes 230 were used to study the effect of pre-oxidized scales on the oxidation behavior of the alloys. The samples were first exposed in air for 24 hours. A continuous  $\text{Mn}_{1.5}\text{Cr}_{1.5}\text{O}_4$  spinel layer could form on the surface of the samples and it was expected to act as a coating to protect the substrate alloy from further oxidation when it was then exposed in coal syngas. Although  $\text{Mn}_{1.5}\text{Cr}_{1.5}\text{O}_4$  spinel can also form in coal syngas, as discussed in 5.1.1, spinel formed in air is denser and has better oxidation resistance.

The pre-oxidized samples were then classified into two groups for comparison. The first group was continuously exposed in air for 100 more hours and the other one was exposed in coal syngas for 500 hours. The detail is discussed in the following section.

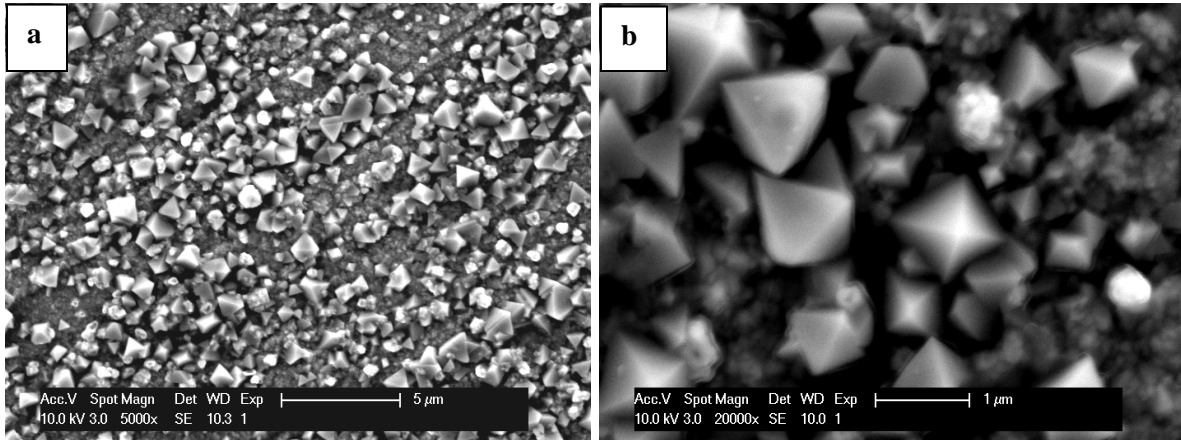
### **Exposed in air for 100 more hours**

Figure 5.7 is the surface morphology of the pre-oxidized Crofer 22 APU samples. EDXS point analysis of particle A in Figure 5.8 showed that it contained 26.33 Wt% Cr, 20.26 Wt% Mn and 5.12 Wt% Fe. The content of Cr was higher than the average Cr content on the surface (13.01 Wt%). The pyramid-like particle should be  $Mn_{1.5}Cr_{1.5}O_4$  spinel. XRD revealed that  $Cr_2O_3$  chromia and some Fe-based phase (s) also existed in the oxide scale.

This is the typical morphology and composition of the scale of Crofer 22 APU when it is exposed in air for a short time. Yang et al [36] used in situ XRD to study the oxidation process of Crofer 22 APU at 800 °C in air. They found that both chromia and spinel were present after 2 hours of oxidation. It appeared that there were preferred orientations of growth of chromia and spinel crystals in the scale. With increasing of time, this texturing diminished, and the crystallographic orientations of the spinel became more homogeneous. As the time increased to 300 hours, the contrast between the spinel and chromia was hardly discernible. After 900 hours, the scale surface was even smoother and the angular spinel crystals had almost totally disappeared, evolving into a fine, agglomerated microstructure. This is to some extent confirmed by our experiment.

Figure 5.9 (a) is the surface SEM image of the sample exposed in air for 100 more hours. We can see that when compared to Figure 5.7, the edges and angles of the spinel particles tended to disappear and the shape became round. A closer observation, as shown in Figure 5.9 (b),

revealed that some of the round particles consisted of many small grains. However, there still were some particles with well-defined pyramid-like shape.



**Figure 5.7:** SEM morphology of the surface of pre-oxidized Crofer 22 APU sample:

(a) 5000X, (b) 20000X

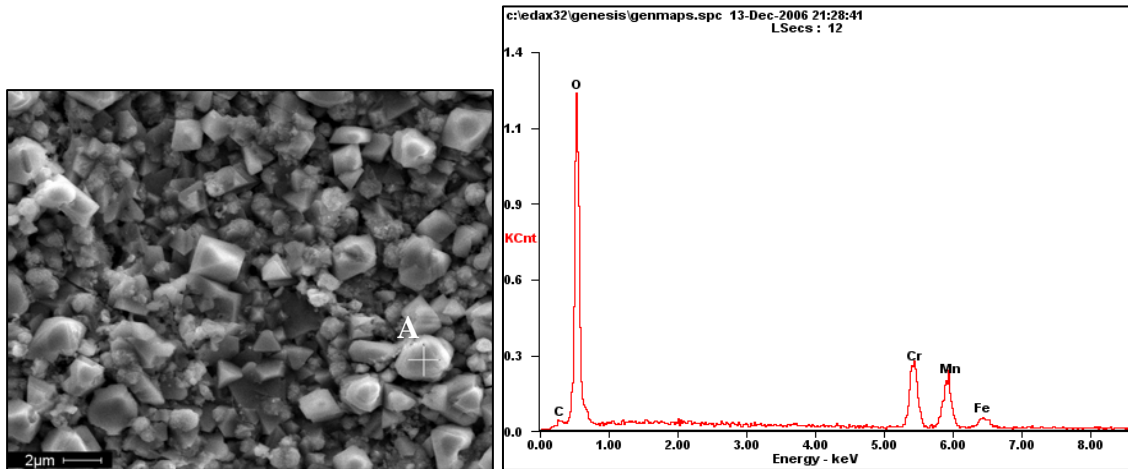


**Figure 5.8:** EDX point analysis of the scale of Crofer 22 APU after further oxidation in air for 100 hours

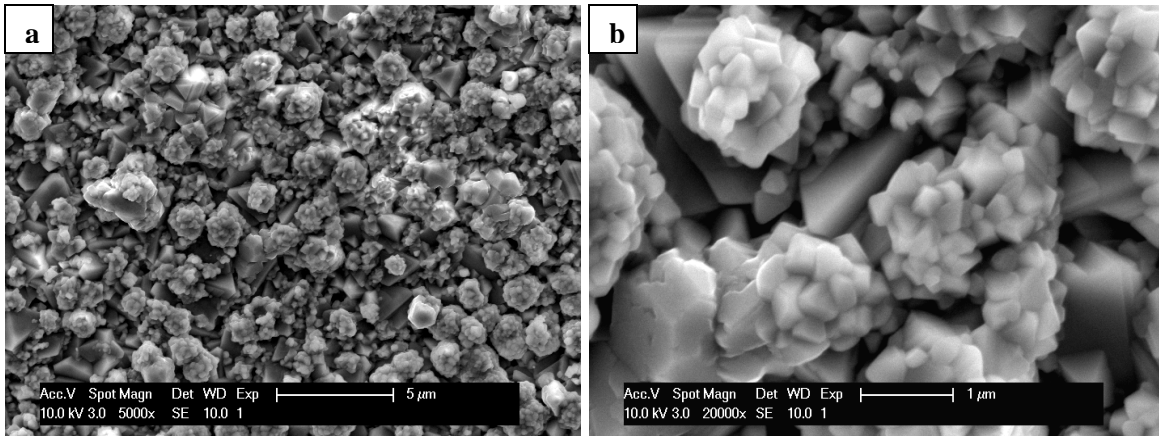
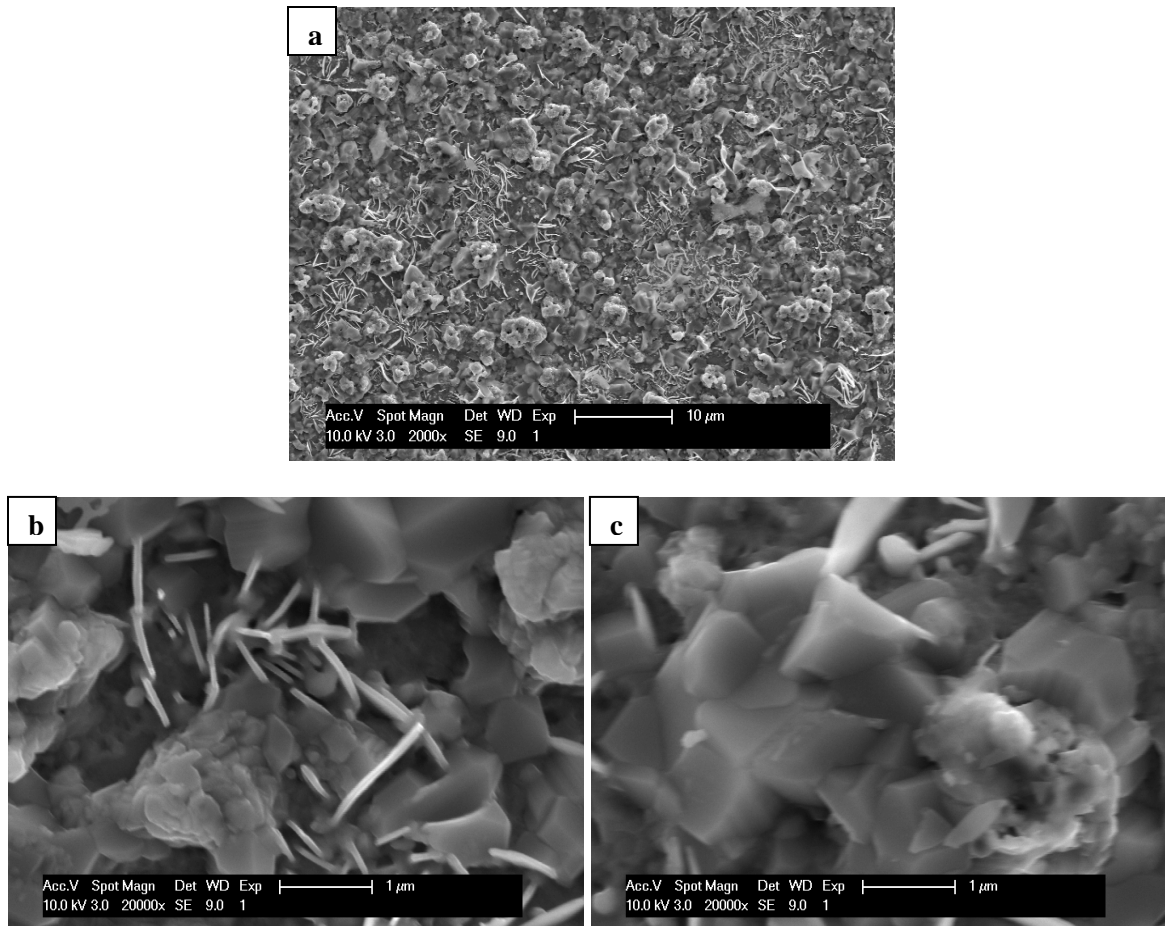


**Figure 5.9:** SEM morphology of the surface of the pre-oxidized Crofer 22APU after further oxidation in air for 100 hours: (a) 5000X, (b) 20000X

### Exposed in coal syngas for 500 more hours

The surface microstructure of the pre-oxidized sample after further oxidation in coal syngas for 500 more hours, as shown in Figure 5.10, was different from that of the scale without pre-oxidation, as shown in Figure 5.4. The surface scale of pre-oxidized sample contained a phase of short-fiber. The very similar short-fiber structure formed on the surface of Crofer 22 APU after oxidation at 800 °C for 300 hours in moist hydrogen (97% $H_2$ /3% $H_2O$ ) was reported to be rich in Mn and Cr and was most likely a spinel phase [36]. This short-fiber was about 1  $\mu m$  in length and grew outward from the prism-like phase. Not all prism-like phase grains had this kind of short fibers on the surfaces. An example of an area where no short-fiber phase existed is given in Figure 5.10 (c).

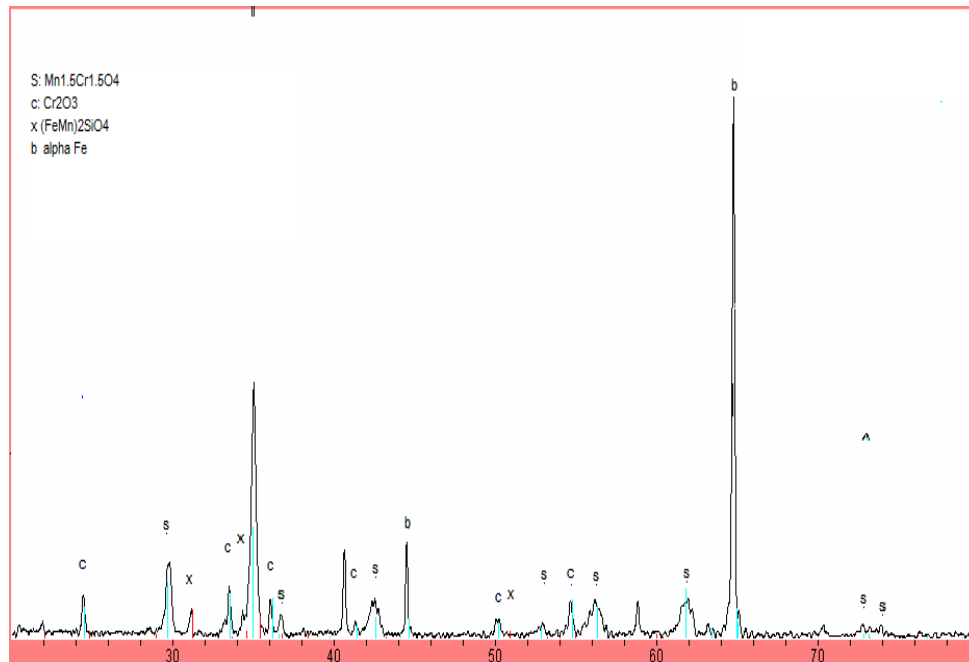
The surface XRD analysis result is given in Figure 5.11. The oxide scale also consisted of  $Mn_{1.5}Cr_{1.5}O_4$  spinel,  $Cr_2O_3$  chromia, and  $(Mn,Fe)_2SiO_4$ . These were the same as the scale formed on the surface of Crofer 22 after oxidation in syngas for 500 hours without pre-oxidation, as shown in Figure 5.5.



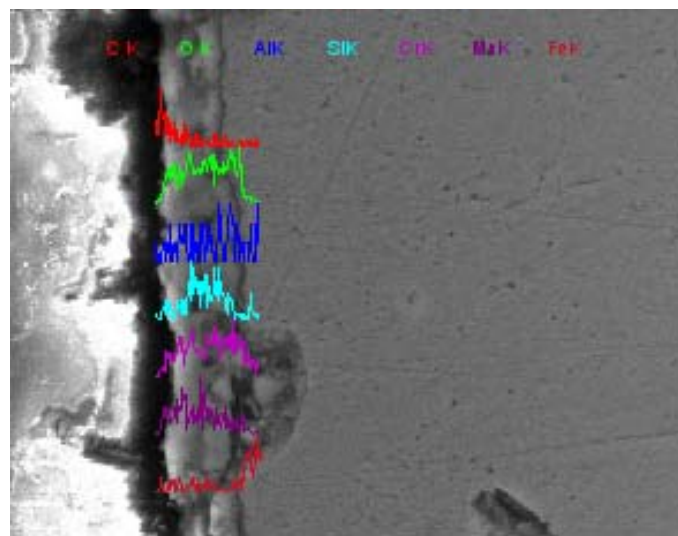
**Figure 5.10:** SEM morphology of the surface of the pre-oxidized Crofer 22APU after further oxidation in syngas for 500 hours: (a) 2000X, (b) 20000X, (c) 20000X (an area without the short-fiber phase)

Figure 5.12 is the SEM cross-sectional microstructure and elemental distributions of the sample. The elements of Mn, Cr, and O were homogeneously distributed through the thickness of the oxide scale. This is similar to the homogeneous scale formed on the sample after oxidation in coal syngas for 500 hours without pre-oxidation (Figure 5.6).

The scale was about 3  $\mu\text{m}$  in thickness, while the scale of the sample without pre-oxidation was about 5.5  $\mu\text{m}$  thick. This provided direct evidence that pre-oxidation is beneficial to the oxidation resistance of the alloy.



**Figure 5.11:** XRD pattern of scales grown on pre-oxidized Crofer 22 APU after further exposure in coal syngas for 500 hours



**Figure 5.12:** EDX linear analysis of the cross section of the oxide scale of pre-oxidized Crofer 22 APU after further exposure in syngas for 500 hours

In summary, no matter pre-oxidation or not, the main phases of scale of the samples were the same, i.e.,  $Mn_{1.5}Cr_{1.5}O_4$  spinel and  $Cr_2O_3$  chromia, and little  $(Mn,Fe)_2SiO_4$ . When the exposure time was up to 500 hours, the boundary between spinel and chromia was indiscernible and these phases would be homogeneously distributed in the scale. Even though, the surface morphology and grain shape of the scales were quite different, see Figure 5.4 and Figure 5.10. It is not clear which kind of morphology is of better oxidation resistance. However, the scale of pre-oxidized sample was much thinner than that of the sample without pretreatment. In this sense, pre-oxidation is an efficient way to improve the oxidation resistant property. Moreover, no internal oxidation zone existed on the surface of the pre-oxidized substrate alloy, although there were some small oxidation areas, which are represented by black spots on the cross section as shown in Figure 5.12.

## **5.2 E-BRITE**

### **5.2.1 Exposed in coal syngas for 100 hours**

The SEM morphology of the surface of the E-Brite sample after oxidation in coal syngas for 100 hours is shown in Figure 5.13. The surface of the scale consisted of nodules with a size varying from several microns to a very small scale. The surface was not smooth and dense. Figure 5.13 (b) is the high magnification SEM image of the surface. We can see that even the nodules themselves were not dense and had short fibers on the surfaces. These nodules were much similar with the structure found at the air side surface of austenitic AISI 304 during simultaneous exposure to dual atmosphere exposure conditions at 800 °C [39].

The XRD pattern of the surface, as shown in Figure 5.14, revealed that the oxide scale mainly consisted of  $Mn_{1.5}Cr_{1.5}O_4$  spinel, and  $Cr_2O_3$  chromia.

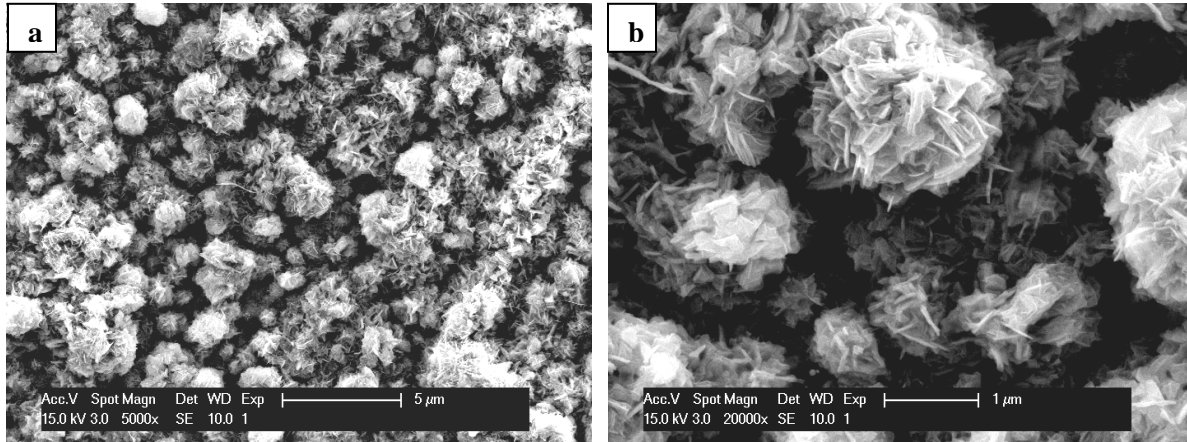


**Figure 5.13:** SEM morphology of the surface of E-Brite after oxidation in coal syngas for 100 hours: (a) 5000X, (b) 20000X

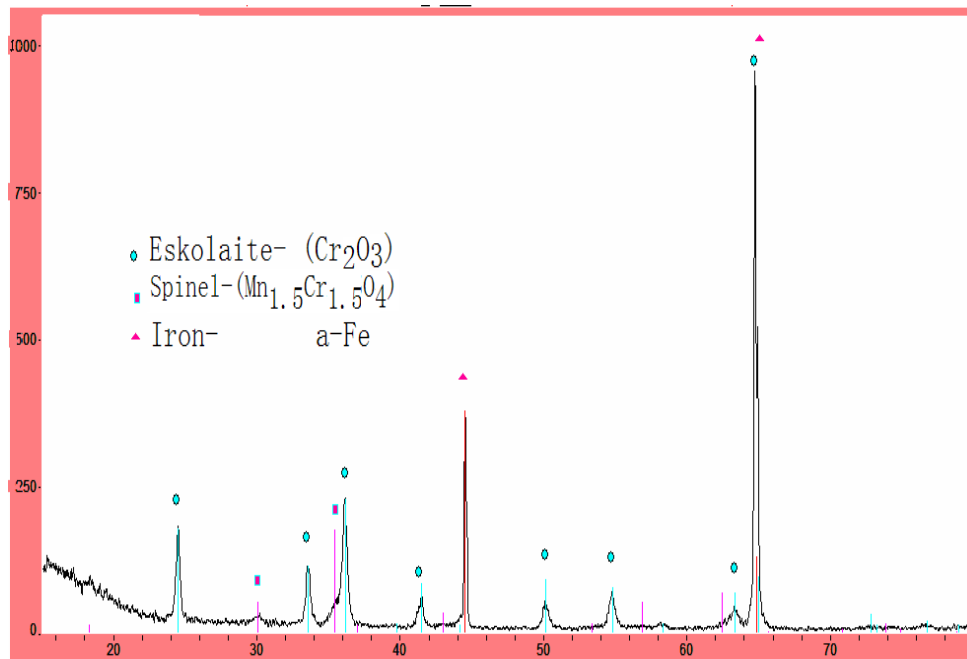


**Figure 5.14:** XRD pattern of scales on E-Brite after oxidation in coal syngas for 100 hours

### 5.2.2 Exposed in coal syngas for 500 hours

Compared to the scale surface of E-Brite exposed in coal syngas for 100 hours, the scale formed for 500 hours were much denser and more homogenous, as shown in Figure 5.15. The nodule structure was not present for this group of samples.

Figure 5.16 is the XRD pattern of the surface, as that for the sample oxidized for 100 hours,  $Mn_{1.5}Cr_{1.5}O_4$  spinel and  $Cr_2O_3$  chromia were the main phases of the oxide scale. Although from the cross-sectional morphology of the scale (Figure 5.17 (a)), it looks that the scale had two layers, EDXS linear analysis found (Figure 5.17 (b)) that Mn, Cr and Si were almost homogeneously distributed in the scale through the thickness.

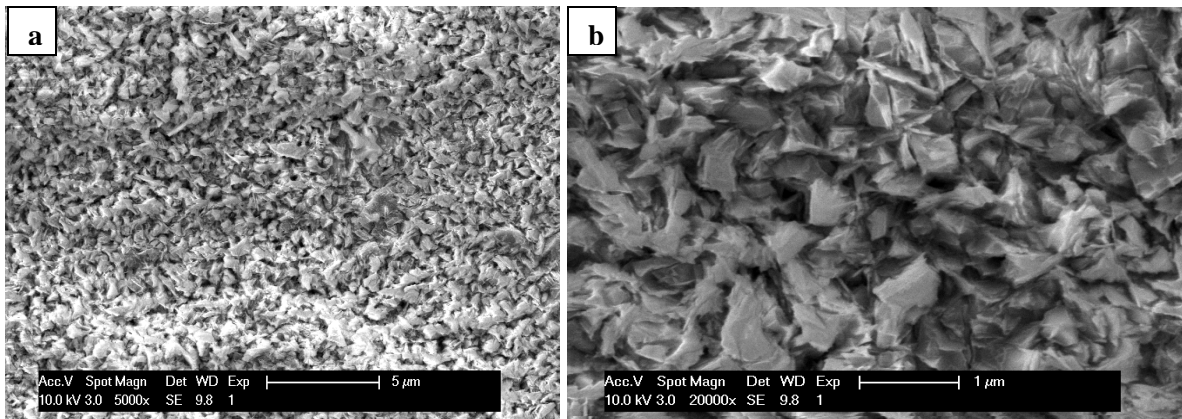


**Figure 5.15:** SEM morphology of the surface of E-Brite sample after oxidation in coal syngas for 500 hours: (a) 5000X, (b) 20000X

The thickness of the scale was less than  $2 \mu m$ , which was much thinner than that of Crofer 22 APU oxidation under the same conditions. This was consistent with the result of Geng et al [18]. They compared the oxidation resistance of several ferritic alloys, including Crofer 22

APU and E-Brite, in air at 800 °C for 500 hours. They found that the oxidation resistance of E-Brite was the best and the mass gain of E-Brite was less than half of that of Crofer 22 APU.

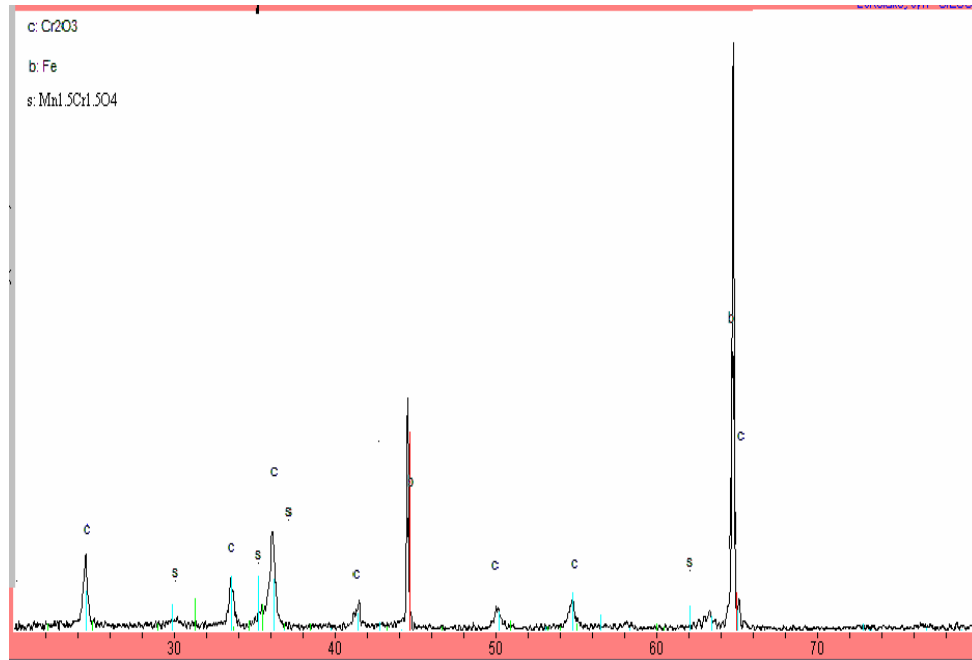


**Figure 5.16:** XRD pattern of scales grown on E-Brite after oxidation in coal syngas at 800 °C for 500 hours

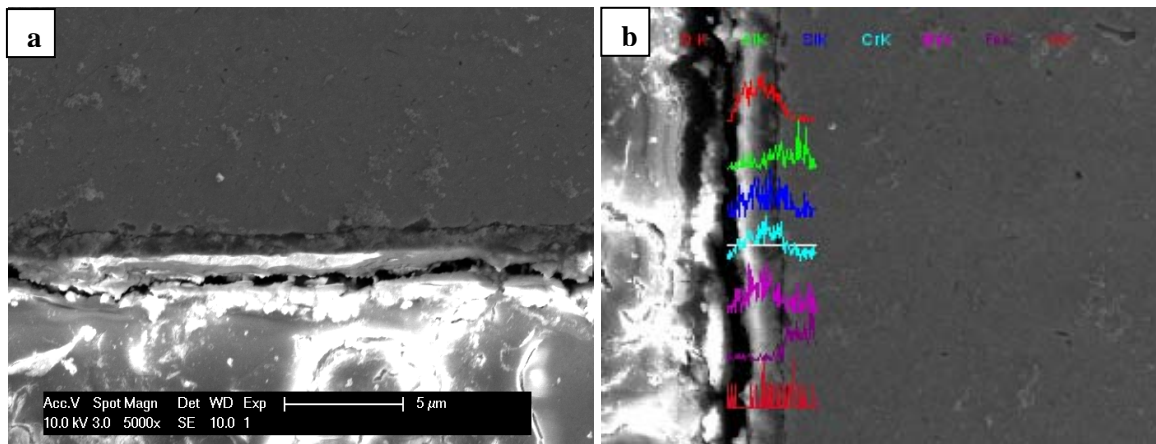


**Figure 5.17:** (a) SEM morphology of the cross section of E-Brite exposed in coal syngas at 800 °C for 500 hours; (b) Cross-sectional EDX linear analysis.

## 5.3 HAYNES 230

### 5.3.1 Exposed in coal syngas for 100 hours

Figure 5.18 shows the SEM morphology of the surface oxide scale of Haynes 230 exposed in coal syngas at 800 °C for 100 hours. The scale consisted of leafy grains as well as a small whisker-like phase. The surface was quite dense and was expected to be of good oxidation resistance.  $\text{Cr}_2\text{O}_3$  chromia,  $\text{Mn}_{1.5}\text{Cr}_{1.5}\text{O}_4$  spinel,  $\text{FeNi}_3$  and  $\text{Fe}_2\text{C}$  were detected by XRD in the scale, as shown in Figure 5.19.  $\text{Cr}_2\text{O}_3$  chromia appeared to be the dominant component in the scale, which was indicated by the high Cr content in the XRD pattern. The weak peaks of spinel indicated that the amount of the spinel phase in the scale was small.

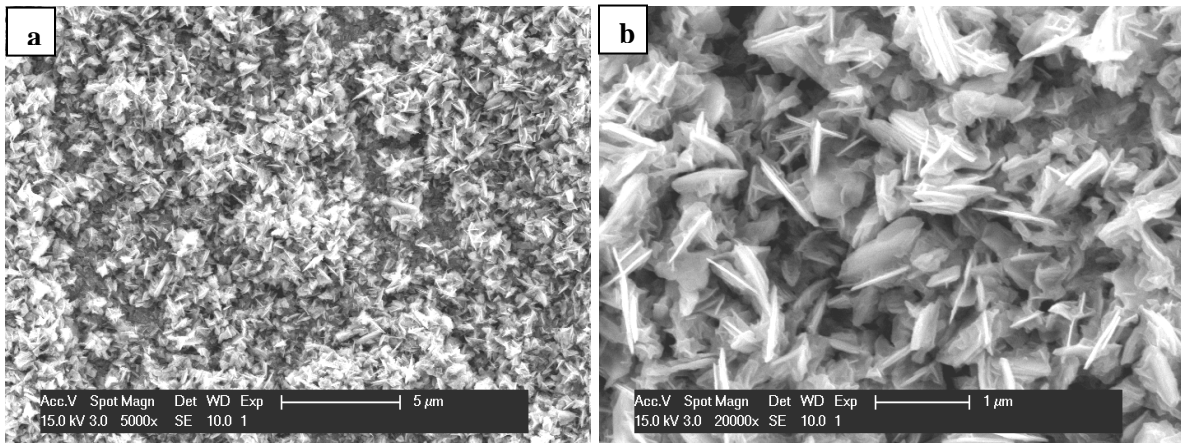


**Figure 5.18:** SEM morphology of the surface of Haynes 230 sample after oxidation in coal syngas for 100 hours: (a) 5000X, (b) 20000X

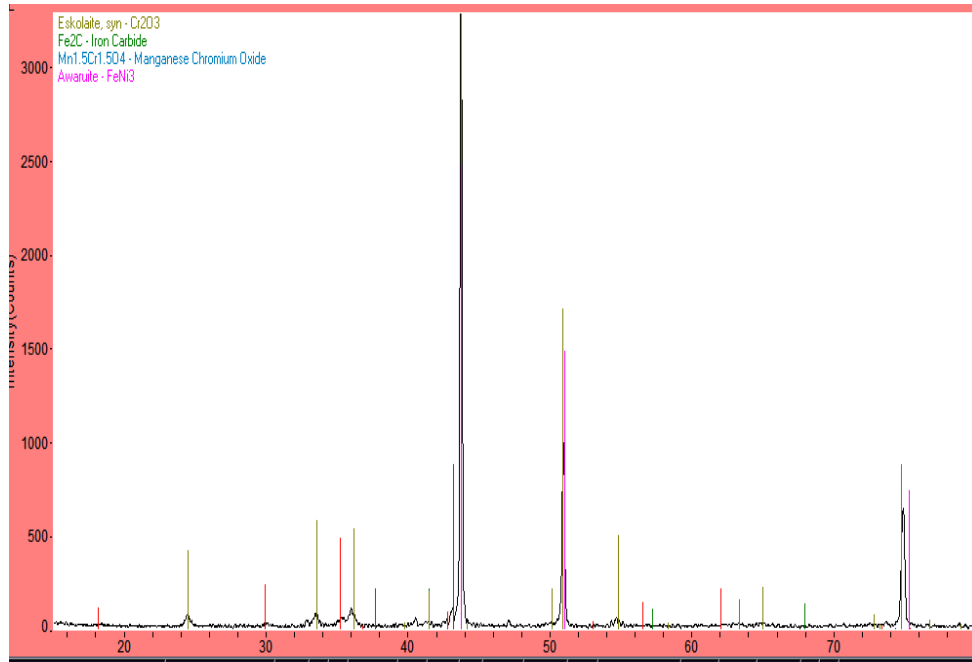


**Figure 5.19:** XRD pattern of scales grown on Haynes 230 sample after oxidation in coal syngas at 800 °C for 100 hours

### 5.3.2 Exposed in coal syngas for 500 hours

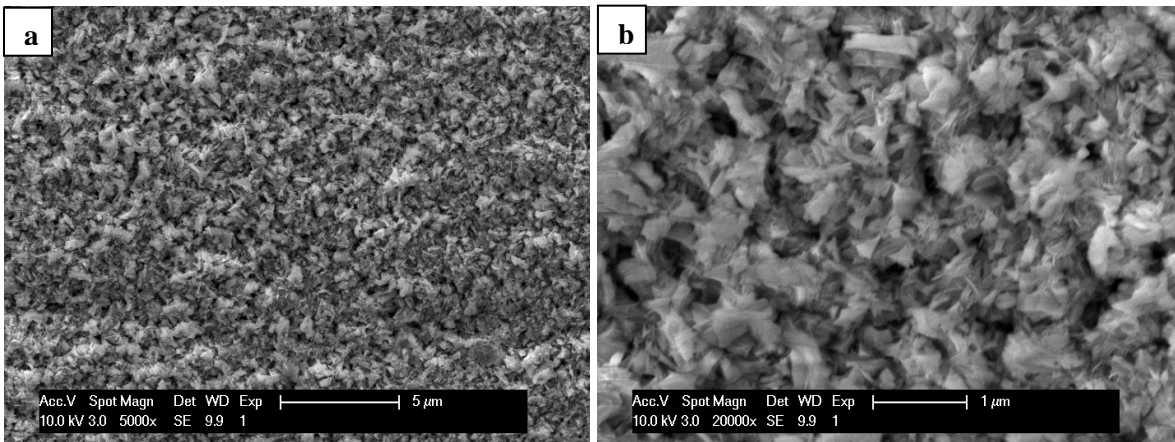


**Figure 5.20:** SEM morphology of the surface of Haynes 230 after oxidation in coal syngas for 500 hours: (a) 5000X, (b) 20000X

When compared to the scale of Haynes 230 oxidized in coal syngas for 100 hours, the scale formed after an exposure of 500 hours was even denser, as shown in Figure 5.20. The whisker- and leafy grains, as shown in Figure 5.18, disappeared. The sample exposed for 500 hours had a smaller and more homogeneous grain and the grain boundaries were hardly discernable.

The XRD pattern, given in Figure 5.21, shows the main phase of the scale of Haynes 230 was  $\text{Cr}_2\text{O}_3$  chromia and the amount of  $\text{Mn}_{1.5}\text{Cr}_{1.5}\text{O}_4$  spinel must be small, which were indicated by their peaks, respectively. A small amount of  $\text{B}_6\text{O}$  was also detected by XRD. The effect of the  $\text{B}_6\text{O}$  phase on the oxidation resistance of the scale is not clear.

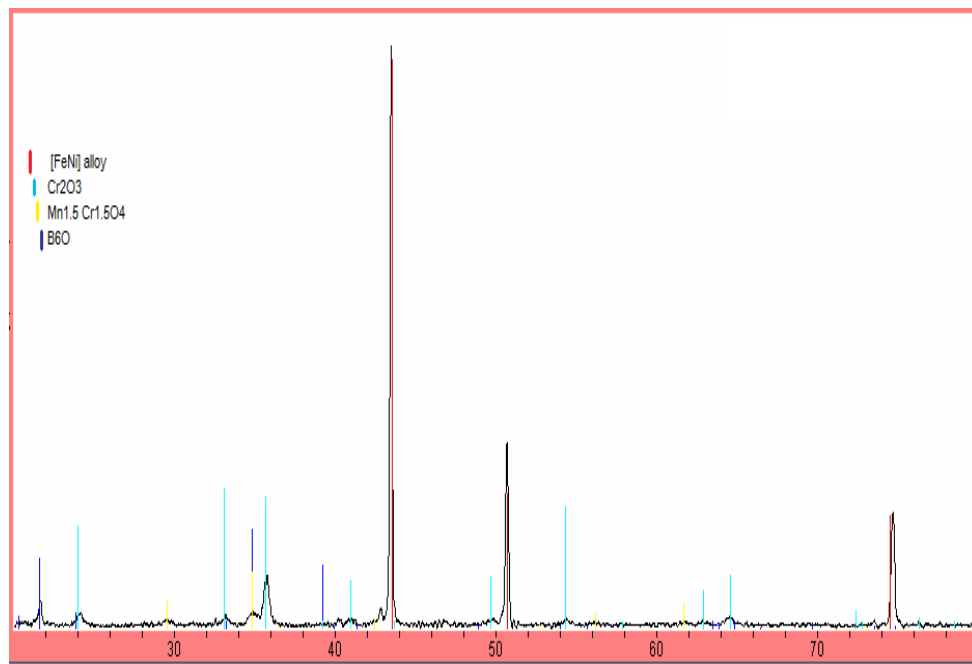


**Figure 5.21:** XRD pattern of scales grown on Haynes 230 after oxidation in coal syngas for 100 hours

Figure 5.22 shows the SEM morphology of the cross section. We can see that the scale was about  $8\ \mu\text{m}$  thick, which was thicker than that of E-Brite and Crofer 22 APU under the same

oxidation conditions. However, the scale was very dense and had good adhesion with the substrate. Although it was thick, this kind of dense and continuous scale could effectively protect the substrate from further oxidation

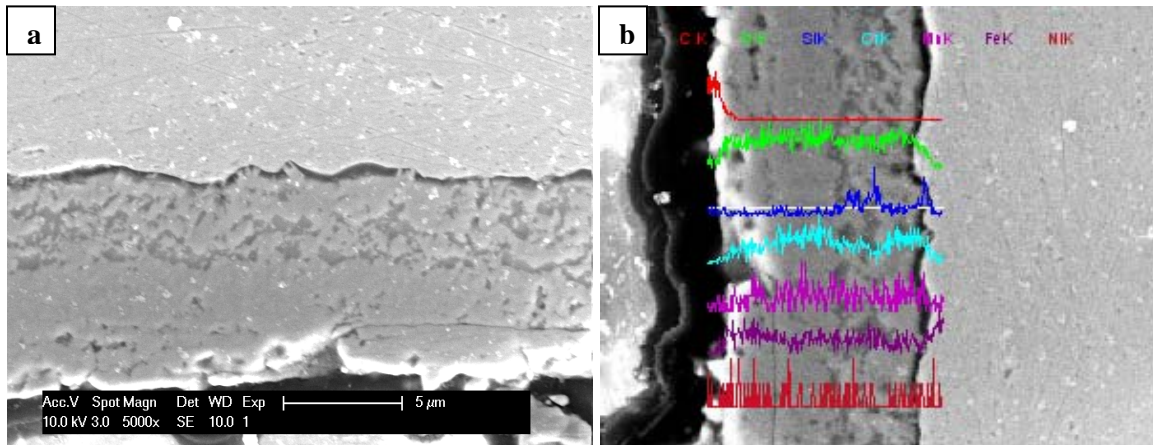


**Figure 5.22:** (a) SEM morphology of the cross section of Haynes 230 exposed in coal syngas at 800 °C for 500 hours; (b) Cross-sectional linear EDX analysis.

The elements of Cr, Mn, Ni and O were almost homogeneously distributed in the scale, as shown in Figure 5.22 (b). The element of C was not detected here and Si seemed to distribute in the inner layer of the scale. It is interesting to notice that the surface of the layer where Si distributed was not as smooth as the outer layer. The presence of Si may impart a positive effect on the oxidation resistance of ferritic steels [18]. Evans et al [40] reported that appropriate amount of Si, which formed silica interlayer between the outer oxide scale and the metal substrate, could optimize the oxidation resistance of nitrated 20Cr-25Ni stainless steels. In this case, it was deduced that the oxidation process would be controlled by chromium-ion diffusion through the silica layer, which acted as a diffusion barrier. However, whether this surface morphology is really related to Si distribution is not clear.

### 5.3.3 Pre-oxidized samples

As the pre-treatment did on Crofer 22 APU, some Haynes 230 samples were pre-oxidized in air for 24 hours to form an oxide scale and then exposed in coal syngas for 500 more hours. Figure 5.23 shows the surface morphology of a pre-oxidized sample after further oxidation in syngas. The scale was denser than that of the sample without pre-oxidation and had less porosity. The grains of two kinds of scales were also different from each other. The grains of the scale without pre-oxidation were quite homogeneous and the grain boundaries were hard to discern. However, the grains of the pre-oxidized scale had prism-like grains with a size up to  $1\ \mu\text{m}$ , which were similar to the grains of the scale formed on the pre-oxidized Crofer 22 APU but without the short-fiber phase (Figure 5.10).

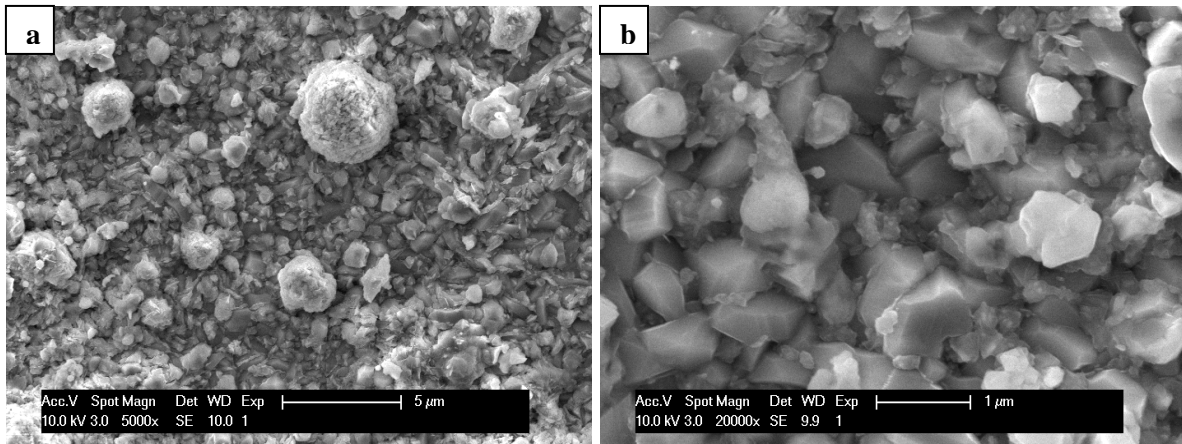


**Figure 5.23:** SEM morphology of the surface of pre-oxidized Haynes 230 after further oxidation in coal syngas for 500 hours: (a) 5000X, (b) 20000X

Figure 5.24 is the XRD analysis result of the scale surface.  $\text{Cr}_2\text{O}_3$  chromia was still the main phase of the scale and the peak of  $\text{B}_6\text{O}$  detected on the scale without pre-treatment did not

appear in the XRD pattern of the pre-oxidized sample. The strong peaks of the substrate alloy phase demonstrated that the scale was thin, which was confirmed by the observation of the cross section, as shown in Figure 5.25 (a). The scale was only about 3  $\mu\text{m}$  thick, much thinner than that of the scale without pre-treatment (8  $\mu\text{m}$ ). This means that pre-oxidation in air can effectively improve the oxidation resistance of the oxide scale.

At the same time, it should be noticed that the small areas in the surface layer of the substrate, labeled by white arrows in Figure 5.25 (a), may be resulted from internal oxidation, which did not present for the sample without pre-oxidation. From figure 5.25 (b), we can see that Cr, Mn, Fe and O were also homogeneously distributed in the scale.

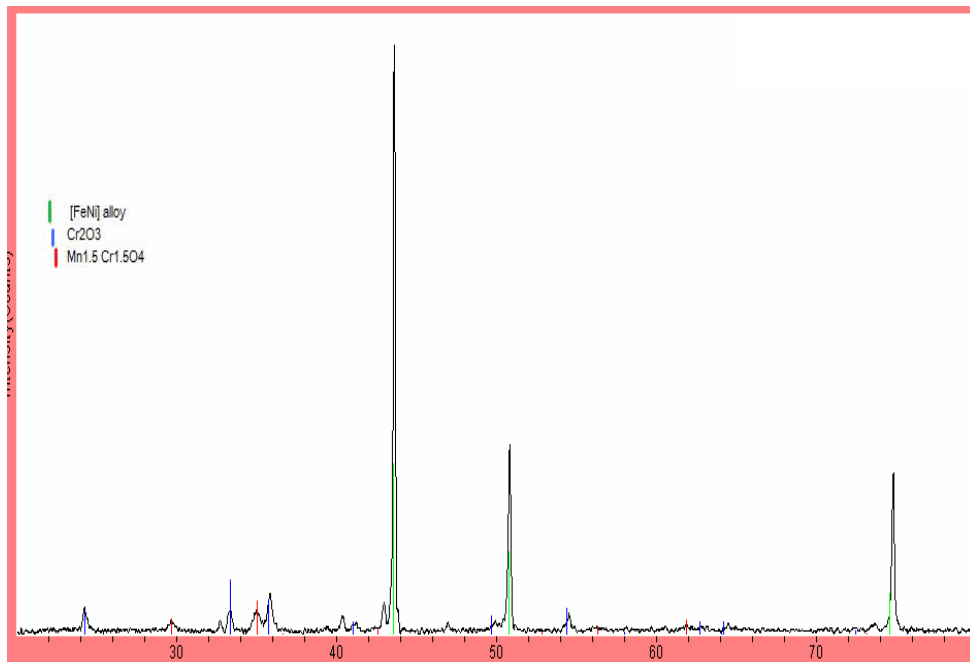


**Figure 5.24:** XRD pattern of scales grown on pre-oxidized Haynes 230 after further oxidation in coal syngas for 500 hours

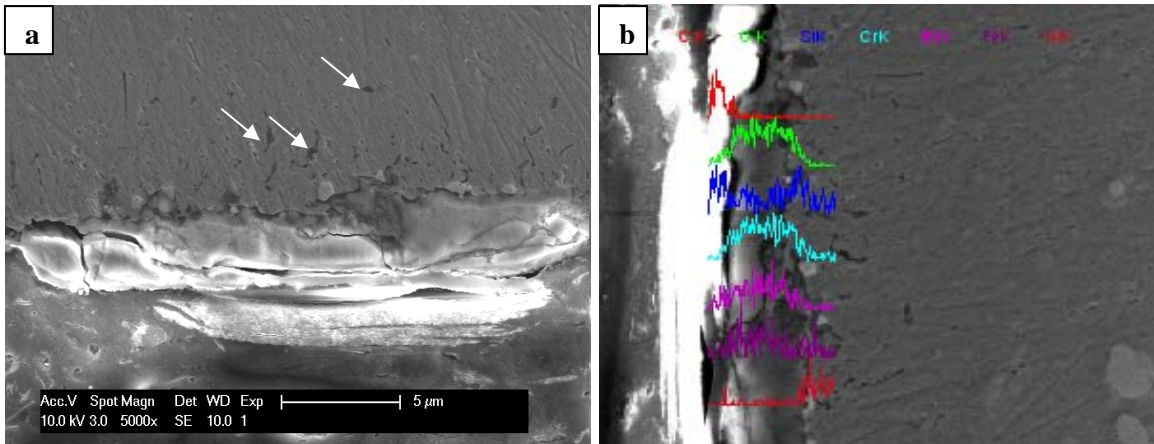


**Figure 5.25:** (a) SEM morphology of the cross section of pre-oxidized Haynes 230 sample after further oxidation in coal syngas for 500 hours; (b) Cross-sectional linear EDX analysis.

In summary, compared to the Haynes 230 sample without pre-oxidation, the pre-oxidized sample had a denser, less porous scale and more homogenous prism-like grains. The scale of the pre-oxidized sample was much thinner than that of the sample without pre-treatment.  $\text{Cr}_2\text{O}_3$  chromia was the main phase of the scale and the amount of  $\text{Mn}_{1.5}\text{Cr}_{1.5}\text{O}_4$  spinel was small for both the samples. These phases were homogeneously distributed in the scale.  $\text{B}_6\text{O}$  was detected in the scale of the sample without pretreatment, while that did not present in the pre-treated sample. As a whole, pre-oxidation in air can effectively improve the oxidation resistance of Haynes 230 at high temperature in coal syngas.

## 5.4 CLAD MATERIALS

As discussed in Chapter 2, cladding can integrate the advantages and avoid the disadvantages of different kinds of alloys and has been expected to produce SOFC interconnect materials of desired oxidation, mechanical and electric properties. In the present

work, E-Brite/Haynes 230 and AISI 430/Haynes 230 clad samples were studied and the oxidation properties were evaluated.

#### 5.4.1 E-Brite/Haynes 230

Figure 5.26 is the surface morphology at the E-Brite side of the E-Brite/Haynes 230 clad sample, which was similar with that of the unclad E-Brite sample oxidized under the same conditions, as shown in Figure 5.13. The scale was dense and the grains were fine. The scales mainly consisted of homogeneously distributed  $\text{Cr}_2\text{O}_3$  chromia and  $\text{Mn}_{1.5}\text{Cr}_{1.5}\text{O}_4$  spinel, as shown in Figure 5.27 and Figure 5.28.

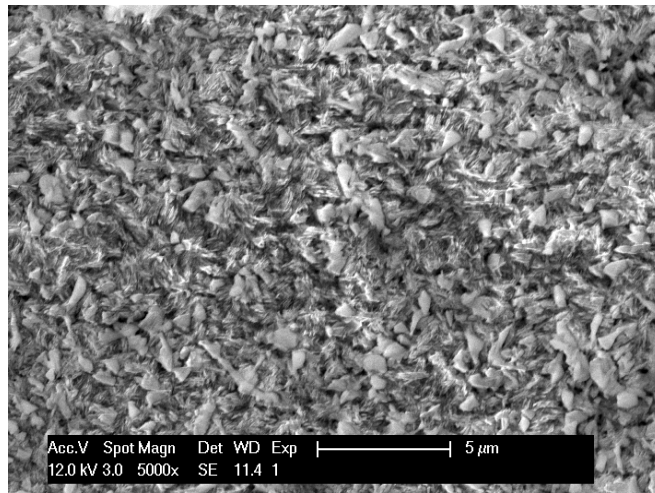


**Figure 5.26:** SEM morphology of the E-Brite side of the E-Brite/Haynes 230 clad sample after oxidation in coal syngas for 500 hours.

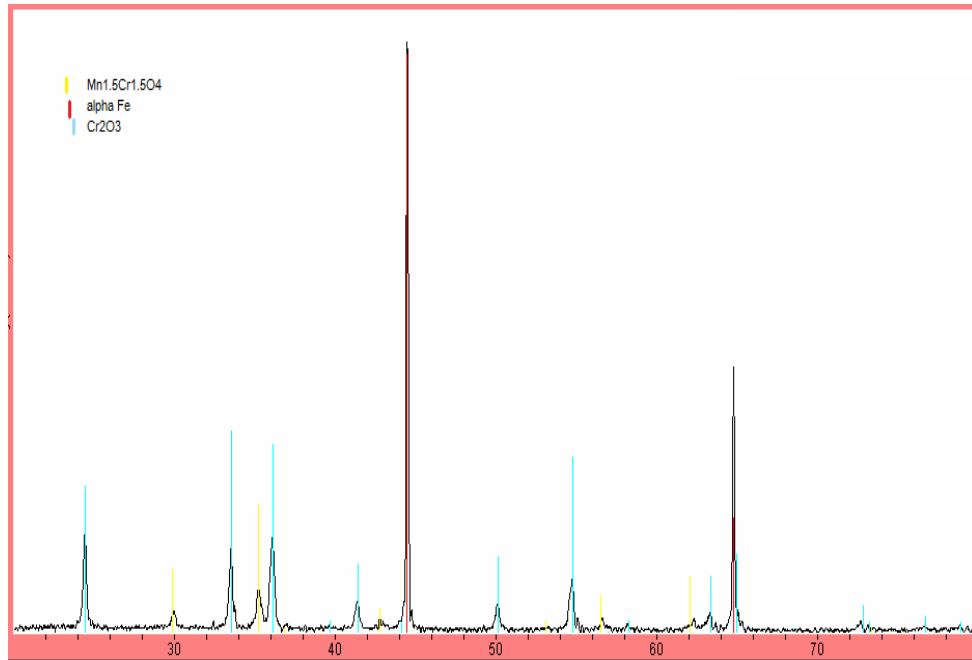


**Figure 5.27:** XRD pattern of scales grown at the E-Brite side of the E-Brite/Haynes 230 clad sample after oxidation in coal syngas for 500 hours.

Moreover, the thickness ( $2 \mu\text{m}$ ) of the scale was almost the same as that of the unclad sample. Although the distribution of the elements such as Mn, Cr, and Fe were the same for clad and unclad E-Brite, Al was only detected in the clad material. Al was reported have a positive effect on the oxidation property of ferritic steels [40].

The surface morphology at the Haynes 230 side is shown in Figure 5.29. Some grains had a prism-like shape. The XRD analysis (Figure 5.30) revealed that the scale of the clad Haynes 230 mainly consisted of  $\text{Cr}_2\text{O}_3$  chromia and a trace amount of  $\text{Mn}_{1.5}\text{Cr}_{1.5}\text{O}_4$  spinel, which was similar with the unclad sample. However, Mo only presented in the scale of the clad sample. Mo played an important role in the development of a complete  $\text{Cr}_2\text{O}_3$  layer in the early stages of oxidation [41]. The presence of Mo oxides at the alloy surface can reduces the oxygen activity, thus favoring formation of a complete chromium oxide layer beneath the initially formed non-protective oxides.

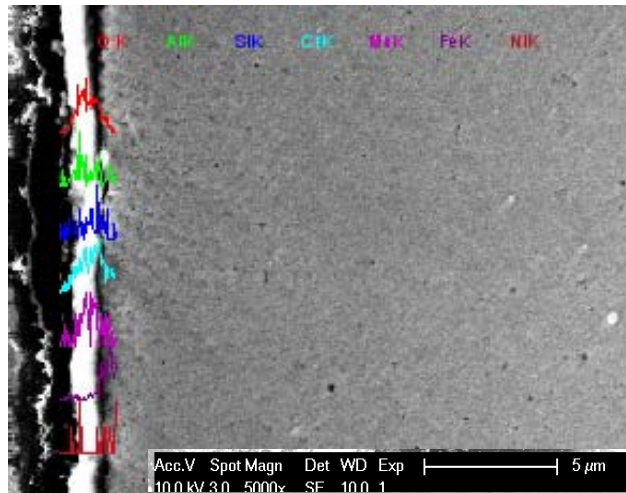


**Figure 5.28:** Cross-sectional EDX linear analysis at the E-Brite side of the E-Brite/Haynes 230 clad sample after oxidation in coal syngas for 500 hours

From Figure 5.31, we can see that the scale was about 3  $\mu\text{m}$  thick, much thinner than that of unclad Haynes 230 (8  $\mu\text{m}$ ) and could be compared with the pre-oxidized sample (about 3  $\mu\text{m}$ ), as shown in Figure 5.22 and Figure 5.25, respectively.

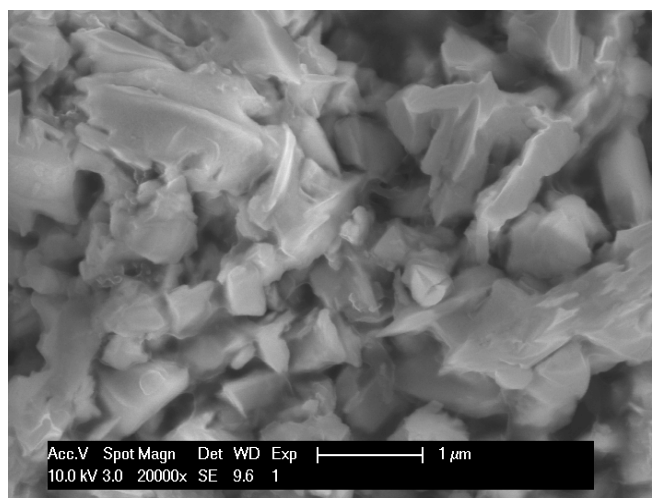


**Figure 5.29:** SEM morphology of the Haynes 230 side of the E-Brite/Haynes 230 clad sample after oxidation in coal syngas for 500 hours.

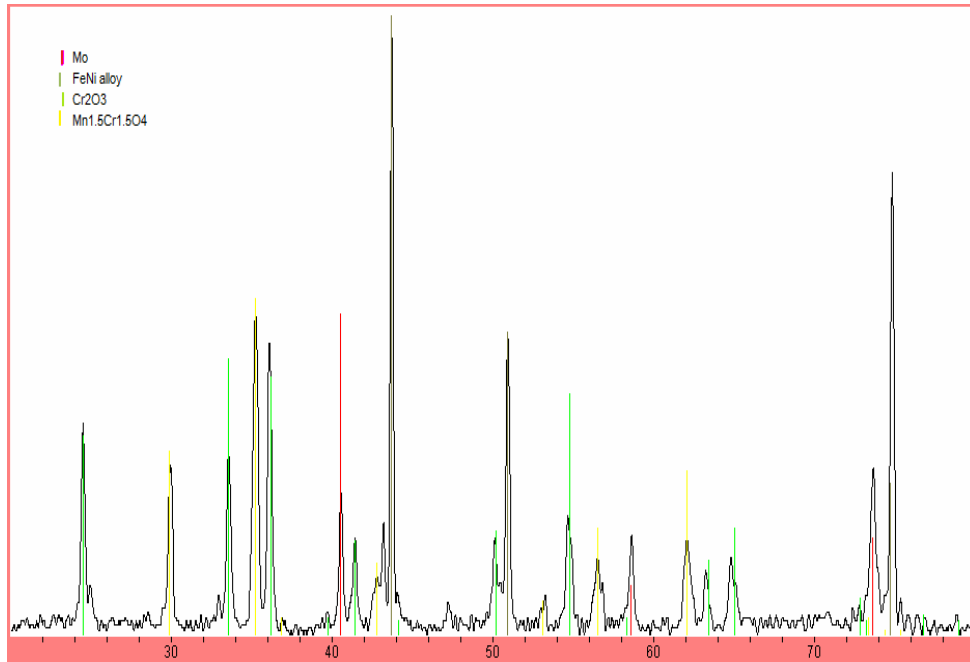


**Figure 5.30:** XRD pattern of scales grown at the Haynes 230 side of the E-Brite/Haynes 230 clad sample after oxidation in coal syngas for 500 hours.

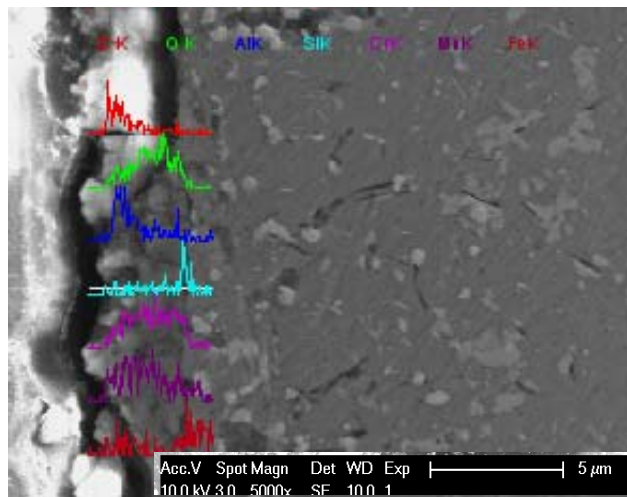


**Figure 5.31:** Cross-sectional EDX linear analysis at the Haynes 230 side of the E-Brite/Haynes 230 clad sample after oxidation in coal syngas for 500 hours

Therefore, although we cannot see significant changes on the oxide scale at the E-Brite side of the clad sample, the thickness of the scale at the Haynes side reduced to half of the

unclad one. Moreover, Mo was detected in the scale of the Haynes 230 side, which could improve the oxidation property of the alloy.

#### 5.4.2 AISI 430/Haynes 230

Figure 5.32 (a) is the surface morphology at the AISI 430 side of the clad AISI 430/Haynes 230 sample. When compared to unclad AISI 430, as shown in Figure 5.32 (b), the morphology had little difference. Both of the sample showed a dense surface consisted of small homogeneous grains but the clad one was smoother.

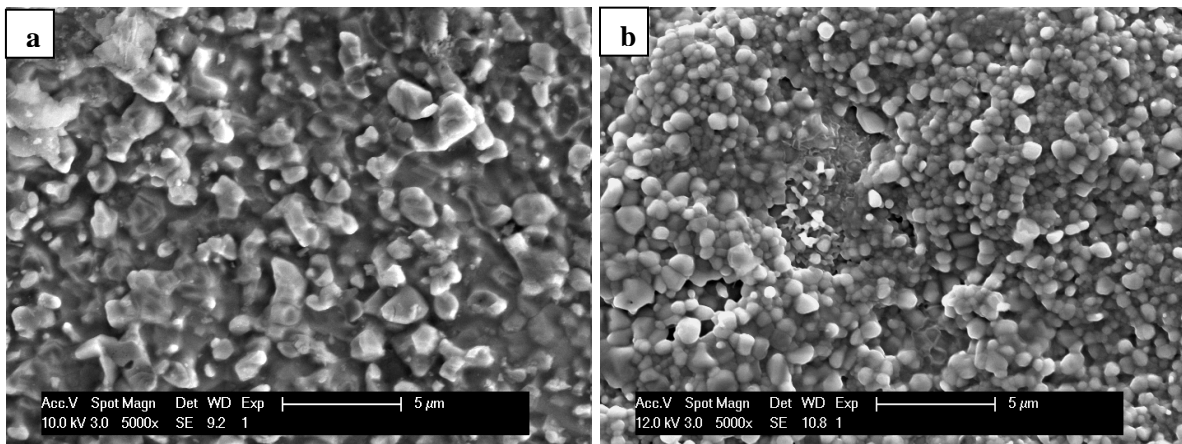


**Figure 5.32:** SEM morphology of AISI 430 after oxidation in coal syngas at 800 °C for 500 hours: (a) clad with Haynes 230, (b) unclad

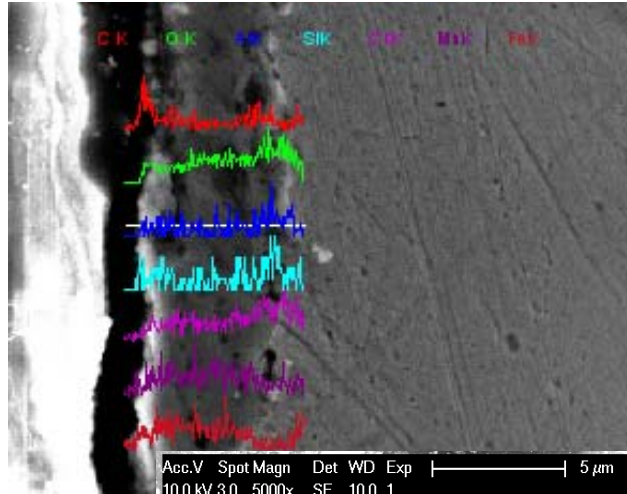


**Figure 5.33:** EDX linear analysis of unclad AISI 430 after oxidation in coal syngas for 500 hours

The main phase of the scale of the unclad AISI 430 were  $\text{Cr}_2\text{O}_3$  chromia and  $\text{Mn}_{1.5}\text{Cr}_{1.5}\text{O}_4$  spinel and they were homogeneously distributed in the scale, as shown in Figure 5.33, which was the case for ferritic steels exposed at high temperature for a long time. However, from the cross sectional EDX analysis (5.34 (a)), we can see that for the clad AISI 430 sample, Mn mainly concentrated in the outer layer of the scale and it should be in the form of  $\text{Mn}_{1.5}\text{Cr}_{1.5}\text{O}_4$  spinel. Therefore, the scale at the AISI 430 sample consisted of two layers. The outer layer was mainly  $\text{Mn}_{1.5}\text{Cr}_{1.5}\text{O}_4$  spinel and the inner layer was  $\text{Cr}_2\text{O}_3$  chromia, which can be clearly seen in Figure 5.34 (b).

This double-layer structure usually forms on the surface of some ferritic alloys after oxidation at high temperature for a short time and when oxidation time increases, the interface between the layers will become indiscernible. Eventually, the two phases will mix up and form a uniform layer [36]. However, the double-layer structure at the AISI 430 side of the clad sample maintained after exposed in coal syngas at high temperatures for 500 hours. Moreover, the scale of the clad AISI 430 ( $1.6 \mu\text{m}$ ) was much thinner than that of the unclad sample ( $5 \mu\text{m}$ ),

as shown Figure 5.34 and Figure 5.33. All of these finding showed that clad with Haynes 230 can significantly improve the oxidation resistance of the scale of AISI 430.

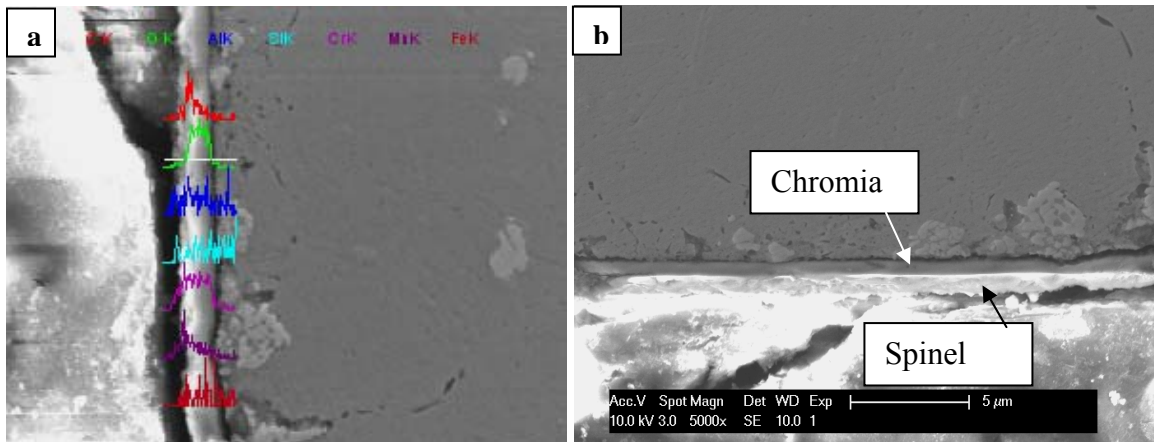


**Figure 5.34:** (a) Cross-sectional EDX linear analysis of the oxide scale at the AISI 430 side of the AISI 430/Haynes 230 clad sample exposed in coal syngas for 500 hours; (b) SEM morphology of the cross section

The surface morphology of the scale at the Haynes 230 side of the clad sample, as shown in Figure 5.35, was different from that of the unclad Haynes 230 (Figure 5.20). The scale of the unclad sample consisted of homogeneous grains and the grain boundaries were hardly discernable. However, the grains at the Haynes 230 side of the AISI 430/Haynes 230 clad sample had a prism-like shape. The prism-like grains were similar to that of the scale of the pre-oxidized Haynes 230 (Figure 5.23) but with a larger size.

Figure 5.36 is the XRD pattern of the scale. Besides the main phases of  $\text{Cr}_2\text{O}_3$  chromia and  $\text{Mn}_{1.5}\text{Cr}_{1.5}\text{O}_4$  spinel, a new phase  $\text{Co}_6\text{W}_6\text{C}$  was also detected. In general, the amount of spinel in the scale of Haynes 230 or other Ni-based alloys is small. However, it is interesting to see that the content of spinel was high in the scale at the Haynes 230 side of the AISI 430/Haynes 230 clad sample.

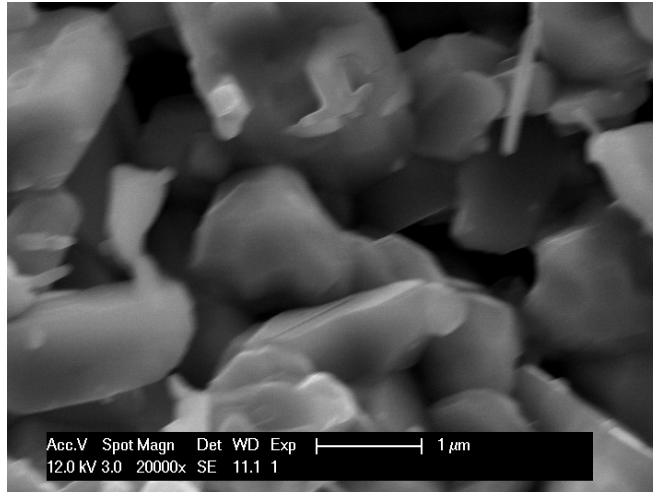


**Figure 5.35:** SEM morphology of the Haynes 230 side of the AISI 430/Haynes 230 clad sample after oxidation in coal syngas for 500 hours.

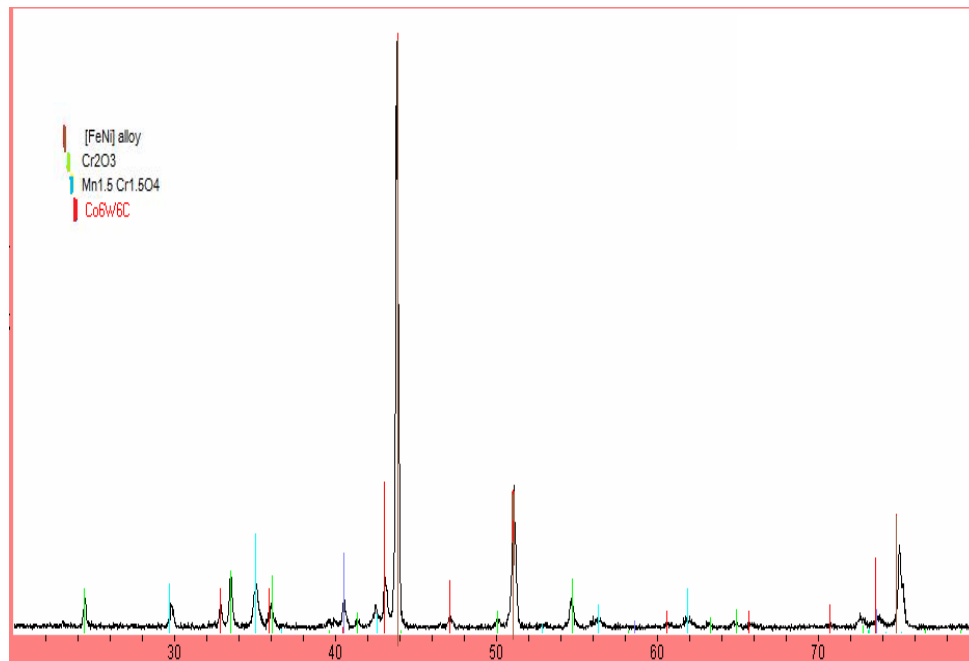


**Figure 5.36:** XRD pattern of scales grown on the Haynes 230 side of the AISI 430/Haynes 230 clad sample after oxidation in coal syngas for 500 hours.

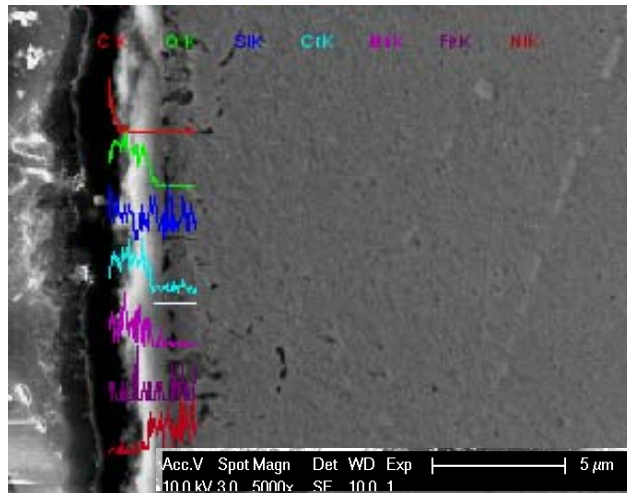


**Figure 5.37:** Cross-sectional EDX linear analysis at the Haynes 230 side of the AISI 430/Haynes 230 clad sample after oxidation in coal syngas for 500 hours

The cross sectional linear EDX analysis (Figure 5.37), shows that the scale at the Haynes side was uniform and the elements were homogeneously distributed in it. The thickness of the scale was about  $1.8 \mu\text{m}$ , several times thinner than that of the unclad Haynes (about  $8 \mu\text{m}$ ) and that of the pre-oxidized sample (about  $3 \mu\text{m}$ ).

A conclusion can be drawn that the oxidation resistance of both AISI 430 and Haynes 230 were improved when they clad together. The thickness of the scales was significantly reduced when compared to the counterpart unclad alloys. Moreover, the content of spinel at the Haynes 230 side was higher than that supposed to be. The scale on the AISI 430 side had a double-layer structure, which was also surprising. These might contribute to the high oxidation resistance of the scales.

## 5.5 SUMMARY AND DISCUSSION

The characteristics of the scales formed on the alloys which were studied in the present work were summarized in Table 5.1. The main phases of the scale of the ferritic alloys were  $\text{Cr}_2\text{O}_3$  chromia and  $\text{Mn}_{1.5}\text{Cr}_{1.5}\text{O}_4$  spinel. The scales of both pre-oxidized and non-pre-oxidized Crofer 22 APU were consisted of prism-like grains, which is a characteristic of  $\text{Mn}_{1.5}\text{Cr}_{1.5}\text{O}_4$  spinel. However, the grains of the scale of E-Brite were leafy and that of AISI 430 was round. The scale of E-Brite was denser and thinner when compared to that of Crofer 22 APU and AISI 430. In this sense, the oxidation resistance of E-Brite was better than that of the other ferritic alloys.

As shown in Figure 5.3, after oxidation in coal syngas for 100 hours, the scale of Crofer 22 APU was a double-layer structure. The outer layer was mainly  $\text{Mn}_{1.5}\text{Cr}_{1.5}\text{O}_4$  spinel and the inner was  $\text{Cr}_2\text{O}_3$  chromia. However, when the time increased to 500 hours, the double-layer structure disappeared, forming a uniform scale in which spinel and chromia were homogeneously distributed. This might be the case for all ferritic alloys. Cox et al. [42] reported that  $\text{Mn}^{2+}$  diffuses faster than  $\text{Cr}^{3+}$  in a  $\text{Cr}_2\text{O}_3$  lattice, leading to a rapid growth of coarse spinel  $\text{Mn}_{1.5}\text{Cr}_{1.5}\text{O}_4$  crystals on the top of a chromia matrix at the early stage of oxidation and eventually resulting in a double-layer scale. With the exposure time increases, the growth rate of spinel will slow down due to the depletion of Mn in the alloy beneath the scale and at the same time dissolves into chromia.

**Table 5.1:** Main characteristic of the scales after oxidation in coal syngas at 800 °C for 500 hours

<b>Samples</b>	<b>Thickness (<math>\mu\text{m}</math>)</b>	<b>Phases</b>	<b>Surface Morphology</b>
<b>Crofer 22 APU</b>	5.5	$\text{Cr}_2\text{O}_3 + \text{Mn}_{1.5}\text{Cr}_{1.5}\text{O}_4$	Prism-like grains, porous surface
<b>Pro-oxidized Crofer 22 APU</b>	3	$\text{Cr}_2\text{O}_3 + \text{Mn}_{1.5}\text{Cr}_{1.5}\text{O}_4$	Prism-like grains with short fiber, dense surface
<b>E-Brite</b>	2	$\text{Cr}_2\text{O}_3 + \text{Mn}_{1.5}\text{Cr}_{1.5}\text{O}_4$	Leafy grains, dense surface
<b>E-Brite (Clad with Haynes 230)</b>	2	$\text{Cr}_2\text{O}_3 + \text{Mn}_{1.5}\text{Cr}_{1.5}\text{O}_4$	Leafy grains, dense surface
<b>AISI 430</b>	5	$\text{Cr}_2\text{O}_3 + \text{Mn}_{1.5}\text{Cr}_{1.5}\text{O}_4$	Round grains, porosity
<b>AISI 430 (Clad with Haynes 230)</b>	1.6	$\text{Cr}_2\text{O}_3 + \text{Mn}_{1.5}\text{Cr}_{1.5}\text{O}_4$	Dense double-layer structure, round grains
<b>Haynes 230</b>	8	$\text{Cr}_2\text{O}_3$ , with little $\text{Mn}_{1.5}\text{Cr}_{1.5}\text{O}_4$ and $\text{B}_6\text{O}$	Small leafy grains, porosity
<b>Pro-oxidized Haynes 230</b>	3	$\text{Cr}_2\text{O}_3$ , with little $\text{Mn}_{1.5}\text{Cr}_{1.5}\text{O}_4$	Prism-like grains with some large nodules
<b>Haynes 230 (Clad with E-Brite)</b>	3	$\text{Cr}_2\text{O}_3$ , with little $\text{Mn}_{1.5}\text{Cr}_{1.5}\text{O}_4$	prism-like grains
<b>Haynes 230 (clad with AISI 430)</b>	1.8	$\text{Cr}_2\text{O}_3 + \text{Mn}_{1.5}\text{Cr}_{1.5}\text{O}_4$ , with little $\text{Co}_6\text{W}_6\text{C}$	Prism-like grains

The scale of Haynes 230 mainly consisted of  $\text{Cr}_2\text{O}_3$  chromia. Although  $\text{Mn}_{1.5}\text{Cr}_{1.5}\text{O}_4$  spinel also existed in the scale, the content was low. The surface morphology of the scale was similar to that of E-Brite. Among all of the alloys studied in the present work, the scale of Haynes 230 (8  $\mu\text{m}$ ) was significantly thicker than that of the ferritic alloys. However, it was reported that the mass gain of Haynes 230 after oxidation in air at 800 °C for 500 hours was several times lower than that of Crofer 22 APU and E-Brite [18, 43], which should result in a thinner scale and better oxidation resistance. The reason for this inconsistency might be caused by the different oxidation media.

Pre-oxidation did improve the oxidation resistance of Crofer 22 APU and Haynes 230. The phases of the scales of both the alloys did not change, while the thickness reduced significantly. The complicated chemical composition of coal syngas, especially the presence of  $\text{H}_2\text{O}$  might

make the alloys easier to be oxidized in coal syngas than in air, and the scale might not as well-developed as in air. Therefore, pre-oxidation in air to form a continuous and fine scale could effectively protect the substrate alloys from further oxidation when then exposed in coal syngas.

From Table 5.1, we can also see that the clad samples showed better oxidation resistance than the corresponding unclad alloys. Although the oxidation resistance of the E-Brite side of the E-Brite/Haynes 230 clad sample did not show many changes, the scale on the Haynes 230 side decreased to 3  $\mu\text{m}$ . Moreover, for the AISI 430/Haynes 230 clad sample, the scales at both sides decreased significantly. The scale at the AISI 430 side had a double-layer structure (the outer layer was  $\text{Mn}_{1.5}\text{Cr}_{1.5}\text{O}_4$  and the inner layer was  $\text{Cr}_2\text{O}_3$ ). As discussed above, this double-layer structure is the typical structure of the scale formed on ferritic alloys after exposed in air or coal syngas for a short time (less than 100 - 200 hours) and when the exposure time increased, the spinel phase will dissolve into the chromia phase and forms a uniform layer. However, this structure was maintained for the clad AISI 430 after oxidation for 500 hours. This is important since the spinel-rich top layer not only protects the chromia-rich layer from evaporation, but also improves the overall scale conductivity. Why this double-layer structure maintained for the clad sample needs further work to clarify.

As for the scale at the Haynes 230 side of the AISI 430/Haynes 230 clad sample, the thickness also decreased and the content of  $\text{Mn}_{1.5}\text{Cr}_{1.5}\text{O}_4$  spinel was higher than it supposed to be. It is interesting because generally, the amount of  $\text{Mn}_{1.5}\text{Cr}_{1.5}\text{O}_4$  in the scale of Ni-based alloys is small, no matter exposed in air, coal syngas, or under dual atmosphere. The high content of spinel  $\text{Mn}_{1.5}\text{Cr}_{1.5}\text{O}_4$  might improve the oxidation resistance of the scale.

It should be noticed that the samples were isothermally exposed in coal syngas in the present experiment. However, in the real operation environment, the interconnects of SOFC are

exposed to air on the cathode side and to fuel on the anode side. Yang et al. [36] compared the oxidation behavior of several ferritic stainless steels in air and under dual exposure conditions and found that the scales grown on the air side under the dual exposure SOFC conditions could be significantly different from scales formed on samples exposed to air on both sides. Nakagawa et al. [44] reported a similar phenomenon upon exposure of a ferritic stainless steel to a dual steam-air environment, in which an outer layer of  $\text{Fe}_2\text{O}_3$  was formed. Therefore, more work is needed to be done under such dual exposure conditions (air on the cathode side and coal syngas on the other side) to evaluate the oxidation properties of the alloys for SOFC interconnect.

Moreover, this work just studied the morphology and phases of the scales. Whether an alloy can be used as SOFC interconnect is dependent on many factors, as discussed in Chapter 1. The coefficient of thermal expansion and electrical conductivity of the scales formed in coal syngas also need further study.

## 6.0 CONCLUSION

The oxidation resistance of Fe-based ferritic alloys Crofer 22 APU, E-Brite, AISI 430 and a Ni-based alloy Haynes 230 exposed in coal syngas at 800 °C for 100 hours and 500 hours was studied. To study the effect of pre-oxidation on the oxidation properties of the alloys in coal syngas, two groups of Crofer 22 APU and Haynes 230 were exposed in air for 24 hours before treated in coal syngas. Moreover, the oxidation behaviors of AISI 430/Haynes and E-Brite/Haynes 20 clad samples were also studied. The results can be concluded as below:

1. For the ferritic alloys, the main phases of the scale were  $\text{Cr}_2\text{O}_3$  chromia and  $\text{Mn}_{1.5}\text{Cr}_{1.5}\text{O}_4$  spinel. At the beginning of oxidation, the spinel phase was on the top of chromia and formed a double-layer structure. With time increased to 500 hours, the double-layer structure disappeared and a uniform scale formed, in which  $\text{Mn}_{1.5}\text{Cr}_{1.5}\text{O}_4$  and  $\text{Cr}_2\text{O}_3$  were homogeneously distributed. Among the ferritic alloys, the scale of E-Brite was the thinnest and expected to have best oxidation resistance in coal syngas, which was consistent with the result in air.

2. The scale of Haynes 230 was thicker than that of the ferritic alloys. The main phase of the scale was chromia  $\text{Cr}_2\text{O}_3$  as well as a trace amount of spinel  $\text{Mn}_{1.5}\text{Cr}_{1.5}\text{O}_4$ .

3. The pre-oxidized samples of Crofer 22 APU and Haynes 230 both had better oxidation resistance when compared to the counterparts without pre-treatment, represented by the thinner thickness. The phases of the scale were not different from that of the un-pretreated samples.

4. The thickness of the scales formed at both sides of the clad samples was significantly decreased, with the exception of E-Brite, whose scale thickness did not change. The scale at the AISI 430 side of the AISI 430/Haynes clad sample had a double-layer structure. This is of great importance due to the outer spinel  $Mn_{1.5}Cr_{1.5}O_4$  layer's protection effect on Cr evaporation when serves under SOFC conditions. What is more, the scale at the Haynes side of the AISI 430/Haynes 230 clad sample had a higher content of spinel  $Mn_{1.5}Cr_{1.5}O_4$ , which might be one of the reasons for good oxidation resistance of the scale.

## BIBLIOGRAPHY

- [1] S. C. Singhal, Solid oxide fuel cells for stationary, mobile, and military applications, *Solid State Ionics*, 2002, 152-153: p.405-410.
- [2] S. M. Haile, Fuel cell materials and components, *Acta Materialia*, 2003, 51: p.5981-6000.
- [3] P. Singh, N. Q. Minh, Solid oxide fuel cells: technology status, *International Journal of Applied Ceramic Technology*, 2004, 1: p.5-15.
- [4] N. Q. Minh, Ceramic fuel cells, *Journal of the American Ceramic Society*, 1993, 76: p.563-588.
- [5] E. Ivers-Tiffée, A. Weber, D. Herbstritt, Materials and technologies for SOFC-components, *Journal of the European Ceramic Society*, 2001, 21: p.1805-1811.
- [6] N. Sammes, *Fuel Cell Technology Reaching Towards Commercialization*. 2006, Springer.
- [7] E. Chen, History. In *Fuel Cell Technology Handbook*, G. Hoogers edited, 2003, CRS Press.
- [8] O. Yamamoto, Solid oxide fuel cells: fundamental aspects and prospects. *Electrochimica Acta*, 2000, 45: p.2423-2435.
- [9] R. M. Ormerod, Solid oxide fuel cells. *Chemistry Society Review*, 2003, 32: p.17-28.
- [10] S. M. Haile, Fuelcell materials and components, *Acta Materialia*, 2003, 51: p. 981-6000.
- [11] “Fuel Cell”, [http://en.wikipedia.org/wiki/Fuel\\_cell](http://en.wikipedia.org/wiki/Fuel_cell), Accessed on October 17, 2007.
- [12] C. S. Song, Fuel processing for low-temperature and high-temperature fuel cells: challenges and opportunities for sustainable development in the 21<sup>st</sup> century, *Catalysis Today*, 2002, 77: p.17-49
- [13] “How fuel cells work”, <http://auto.howstuffworks.com/fuel-cell5.htm>, Accessed on October 18, 2007
- [14] N. Q. Minh, Solid oxide fuel cell technology-features and application, *Solid State Ionics*, 2004, 174: p. 271-277.

- [15] N. Q. Minh, Takahashi, Science and Technology of Ceramic Fuel Cells, 1995, Elsevier.
- [16] W. Z. Zhu, M. Yan, Perspectives on the metallic interconnects for solid oxide fuel cells, Journal of Zhejiang University Science, 2004, 5: p. 1471-1503.
- [17] W. Z. Zhu, S. C. Deevi, Development of interconnect materials for solid oxide fuel cells, Materials Science and Engineering A, 2003, 348: p. 227-243.
- [18] S. J. Geng, J. H. Zhu, Z. G. Lu, Evaluation of several alloys for solid oxide fuel cell interconnect application, Scripta Materialia, 2006, 55: p.239-242.
- [19] J. W. Fergus, Metallic interconnect for solid oxide fuel cells, Materials Science and Engineering A, 2005, 397: p.271-283.
- [20] K. Hilpert, D. Das, M. Miller, D. H. Peck, R. Weiss, Chromium vapor species over solid oxide fuel interconnect materials and their potential for degradation processes, Journal of the Electrochemical Society, 1996, 143: p.3642-3647.
- [21] E. J. Griner, H. W. Kock, in: Proceedings of the first European solid oxide fuel cell forum, Lucerne, Switzerland, 1994, 1:525.
- [22] US Department of Energy (DOE), Fuel Cell Handbook, seventh edition, 2004.
- [23] N. Birks, G. H. Meier, F. S. Pettit, Introduction to the High-Temperature Oxidation of Metals, second edition, 2006, Cambridge University Press.
- [24] S. Laney, Modifying ferritic stainless steels for solid oxide fuel cell applications, PhD Dissertation, University of Pittsburgh, 2007.
- [25] P. Kofstad, High-Temperature Oxidation of Metals, 1966, John Wiley & Sons.
- [26] Z. G. Yang, G. G. Xia, S. P. Simnwe, J. W. Stevenson, Thermal growth and performance of manganese cobaltite spinel protection layers on ferritic stainless steel SOFC interconnects, Journal of the Electrochemical Society, 2005, 152: p.A1896-1901.
- [27] K. Hilpert, W. J. Quadackers, L. Singheiser, Interconnects, in Handbook of Fuel Cells, Volume 4, Fuel Cell Technology and Applications, John Wiley & Sons Ltd., 2003.
- [28] Z. G. Yang, G. G. Xia, J. W. Stevenson,  $Mn_{1.5}Co_{1.5}O_4$  spinel protection layers on ferritic stainless steels for SOFC interconnect applications, Electrochemical and Solid-State Letters, 2005, 8: p.A168-170
- [29] L. Chen, B. Jha, Z. G. Yang, G. G. Xia, J. W. Stevenson, P. Singh, Clad metals by roll bonding for SOFC interconnects, Journal of Materials Engineering and Performance, 2006, 15: p.399-403

- [30] L. Chen, G. Yang, B. Jha, Z. G. G. Xia, J. W. Stevenson, Clad, metals, roll bonding and their applications for SOFC interconnects, *Journal of Power Sources*, 2005, 152: p.40-45.
- [31] Crofer 22 APU: Material data sheet No. 4046, 2006, Thyssenkrupp.
- [32] “Stainless steel E-brite alloy for solid oxide fuel cells”, <http://www.alleghenyludlum.com/ludlum/Documents/E-BRITE%20050207.pdf>, Accessed on October 31, 2007.
- [33] “Haynes 230 alloy”, <http://www.haynesintl.com/pdf/H3060>, Accessed on October 31, 2007
- [34] L. Jian, P. Jian, H. Bing, G. Y. Xie, Oxidation kinetics of Haynes 230 alloy in air at temperature between 650 and 850 °C, *Journal of Power Source*, 2006, 159: p. 641-645.
- [35] D. England, A. Virkar, Oxidation kinetics of some nickel-based superalloy foils and electronic resistance of the oxide scale formed in air, *Journal of the Electrochemical Society*, 1999, 146: p. 3196-3202.
- [36] Z. G. Yang, J. S. Hardy, M. S. Walker, G. G. Xia, S. P. Simner, J. W. Stevenson, Structure and conductivity of thermally grown scales on ferritic Fe-Cr-Mn steel for SOFC interconnect application, *Journal of the Electrochemical Society*, 2004, 151: p.A1825-A1831.
- [37] N. naumenko, J. Le-Coze, E. Wessel, W. Ficher, W. J. Quadackers, Effect of trace amounts of carbon and nitrogen on the high temperature oxidation resistance of high purity FeCrAl alloys, *Materials Transactions*, 2002, 43: p.168-172.
- [38] Z. G. Yang, G. G. Xia, G. D. Maupin, J. W. Stevenson, Conductive protection layers on oxidation resistant alloys for SOFC interconnect application, *Surface and Coating Technology*, 2006, 201: p.4476-4483.
- [39] P. Singh, N. Q. Minh, Solid oxide fuel cells: technology status, *International Journal of Applied Ceramic Technology*, 2004, 1: p.5-15.
- [40] H. E. Evans, D. A. Hilton, R. A. Holm, S. J. Webster, Influence of Silicon additions on the oxidation resistance of a stainless steel, *Oxidation of Metals*, 1983, 19: p.1-18.
- [41] A. Ul-Hamid, A. I. Mohammed, S. S. Al-Jaroudi, H. M. Tawancy, N. M. Abbs, Evolution of oxide scale on a Ni-Mo-Cr alloy at 900 °C, *Materials Characterization*, 2007, 58: p.13-23.
- [42] M. G. C. Cox, B. McEnaney, V. D. Scott, A chemical diffusion model for partitioning of transition elements in oxide scales on alloys, *Philosophical Magazine*, 1972, 26: p.839-851.

- [43] S. J. Geng, J. H. Zhu, Z. G. Lu, Evaluation of Haynes 242 as SOFC interconnect material, *Solid State Ionics*, 2006, 177: p.559-568.
- [44] K. Nakagawa, Y. Mastsunaga, T. Yangisawa, Corrosion behavior of ferritic steels on the air sides of boiler tubes in a steam/air dual environment, *Materials at High Temperatures*, 2003, 20: p.67-73